UNIVERSITÀ DEGLI STUDI DI PALERMO

D012 - Molecular Medicine and Biotechnologies
Department of Biomedicine, Neuroscience and Advanced Diagnostics (Bi.N.D.)
SSD BIO/18

Identification of molecular markers involved in cellular response to aneuploidy in normal and tumor cells

IL DOTTORE
DANILO CILLUFFO

IL COORDINATORE
PROF. MASSIMO MIDIRI

IL TUTOR
PROF. ALDO DI LEONARDO

CICLO XXXII
2020

LIST OF PAPERS

This thesis consists of a publication and one paper in process to be submitted to an international scientific journal as listed below:

- Veneziano Lorena, Barra Viviana, **Cilluffo Danilo**, Di Leonardo Aldo (2019). Proliferation of aneuploid cells induced by CENP-E depletion is counteracted by the $p14^{ARF}$ tumor suppressor. Molecular Genetics and Genomics, 294(1), 149-158.

- **Cilluffo Danilo**, Barra Viviana, Spatafora Sergio, Coronnello Claudia, Contino Flavia, Bivona Serena, Feo Salvatore, Di Leonardo Aldo. Gene expression profiling of aneuploid IMR90 cells induced by RNA interference of pRb, DNMT1 and MAD2. Genomics (2020).

POSTER PRESENTATION

1. **Cilluffo, D**., et al. "The tumor suppressor p14ARF hampers proliferation of aneuploid cells induced by CENP-E partial depletion." XV Congresso FISV 2018.

INTRODUCTION

1 Aneuploidy, CIN and cancer

Aneuploidy is a karyotype alteration that results in changes of chromosome number that is not an exact multiple of the haploid number (2n ± x) and is often caused by errors of chromosome segregation during mitosis. Aneuploidy in an hallmark of cancer cells (Chunduri et al. 2019) indeed, ~90% of solid tumours are aneuploid, and Theodore Boveri proposed a causal role of aneuploidy in tumors development more than a century ago (Boveri 1902; Boveri 1904), over time experimental results have reinforced this idea. By contrast, there has been rather limited progress in understanding how aneuploidy contributes to cancer initiation and progression (Van Jaarsveld et al. 2016).

Moreover, cancer cells show an increased rate of chromosome missegregation due to errors in mitosis called Chromosomal instability (CIN) (Gordon et al. 2012). One of the main products of CIN is aneuploidy, a condition associated with the gain or loss of whole chromosomes or parts of them leading to genomic imbalances (Giam et al. 2015). The causes of CIN and aneuploidy can be many: mitotic slippage, cytokinesis failure, spindle multi-polarity, defective kinetochore-microtubule attachments, perturbed microtubule dynamics, cohesion defects, and impaired Spindle Assembly Checkpoint (SAC) (Thompson et al. 2010; Nicholson et al. 2011).

Chromosomal imbalance caused by aneuploidy is directly correlated to changes in transcript and protein expression levels of genes present on the aneuploid chromosomes, and deregulation of oncogenes and tumor suppressor genes can have direct effects on cellular transformation. Moreover, aneuploidy can lead to CIN by changing the stoichiometry of protein complexes required for genome maintenance or by scaling defects brought about by the presence of extra DNA. At the same time, chromosome missegregation has the potential to increase DNA damage and genomic instability. (Fig.1)

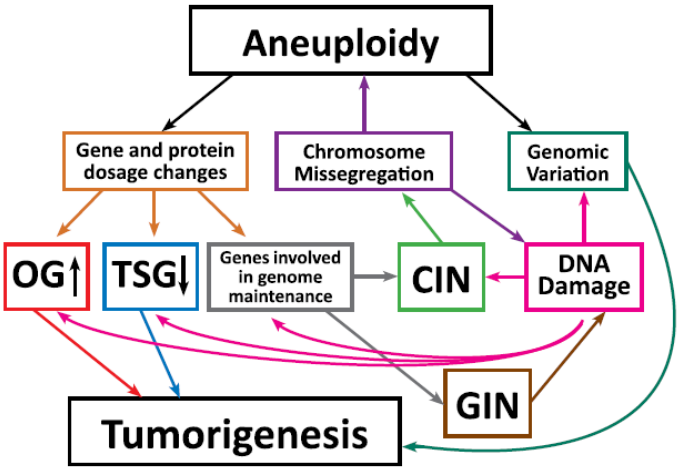

Fig. 1 Relationship scheme between aneuploidy, CIN and tumorigenesis. (OG = oncogene; TSG = tumor suppressor gene; CIN = Chromosome instability; GIN = Genomic instability) (Giam et al. 2011)

It is not clear if CIN and aneuploidy are sufficient to induce pre-neoplastic transformation in normal cells. Both aneuploidy and CIN were associated with patients with poor prognosis, development of metastases (Smid et al. 2011; McGranahan et al. 2012) and acquisition of resistance to chemotherapy (Lee et al. 2011). Many studies on mouse model showed that partial inactivation of proteins involved in the SAC or protein required for proper chromosome alignment results either in increased chromosome missegregation and aneuploidy.

1.1 The Spindle Assembly Checkpoint (SAC)

Mitosis, or phase M of the cell cycle, is the process by which the-division of the mother cell into two genetically identical daughter cells takes place, this process consists of several sub-phases. These phases are prophase, prometaphase, metaphase, anaphase, and telophase. Cytokinesis is the final physical cell division that follows telophase (Fig. 2).

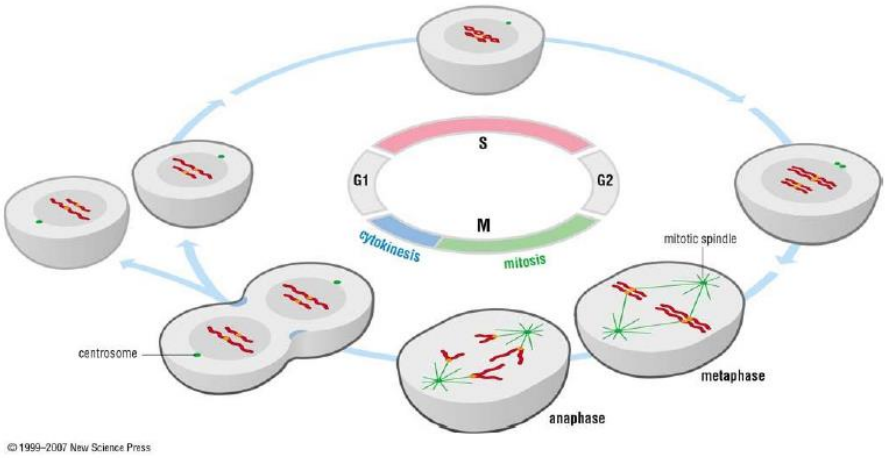

Fig. 2: Schematic representation of the stages of Mitosis and Cell cycle (The Cell cycle: Principles of control David O Morgan)

Mitosis is a critic period of the cell cycle because DNA damage cannot be repaired when the chromosomes are condensed (Rieder & Maiato 2004). Kinetochore attacks to microtubules is a casual event in cell, consequently, all sister chromatids are not captured simultaneously by the spindle fibers. Eukaryotic cells have developed a control mechanism called Spindle Assembly Checkpoint (SAC), which is active both in the absence of a proper strength of kinetochore-microtubule tension and when the kinetochore is not properly attached to the spindle fibers. The SAC prevents entry into anaphase and premature chromosome segregation until all kinetochores are properly attached to the mitotic spindle. The SAC aims to maintain genomic balance by facilitating equal segregation of chromosomes between the two daughter cells.

The SAC is activated in early mitosis to monitor the attachment between microtubules and chromosomes kinetochores working to prevent aneuploidy caused by improper sister chromatid separations. This function is achieved through assembly of the mitotic checkpoint complex (MCC), that assembles from the interaction of the three SAC proteins Mad2, BubR1/Mad3, and Bub3 which inhibits the E3 ubiquitin ligase activity of the anaphase promoting complex/cyclosome (APC/C) CDC20 (Musacchio 2015).

When the SAC is satisfied, the MCC is disassembled and APC/C CDC20 drives ubiquitination and degradation of cyclin B1 and securin. These events induce mitotic exit and sister chromatid separation by degradation of the cohesin complex.

The improper or absent attachment of even a single chromosome with the spindle microtubules generates a STOP signal which activates the SAC and prevents the metaphase-anaphase transition to help the cell to provide the time needed for all kinetochores are captured by the spindle fibers with the development of proper tension (Silva et al. 2011). However, the SAC activation in a cell depends on the presence of at least one of the following: the number of unattached kinetochores (Dick & Gerlich 2013), the amount of mitotic arrest deficient 2 (Mad2) protein at the unattached kinetochores, the amount of Mitotic Checkpoint Complex (MCC) formed (Fig. 3) (Collin et al. 2013).

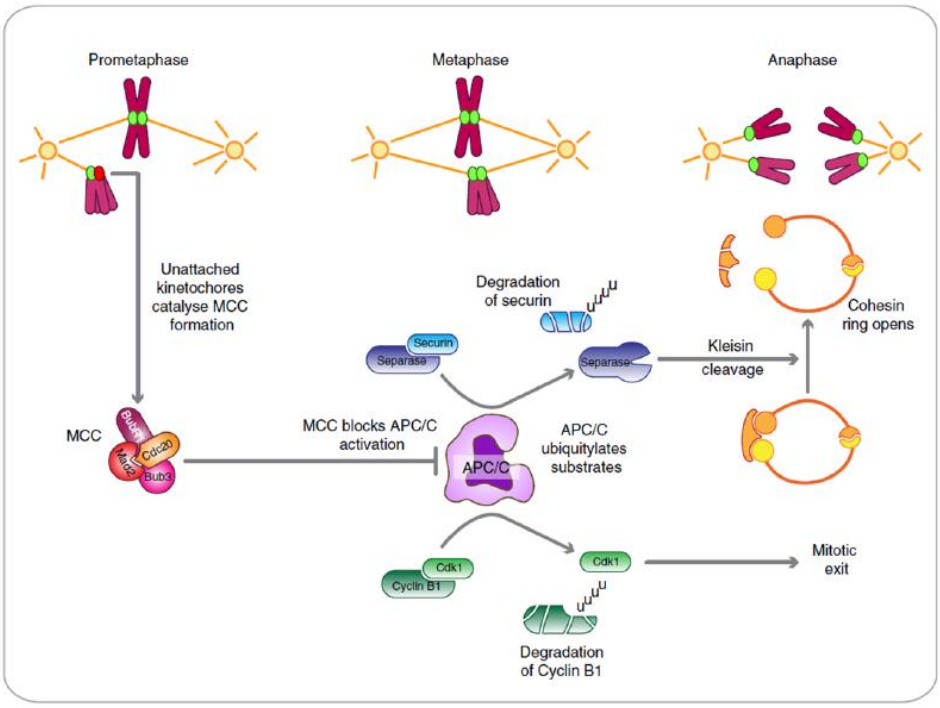

Figura 3: Schematic representation of the spindle assembly checkpoint (Lara-Gonzalez et al. 2012)

A weakened SAC may allow cells to enter anaphase in the presence of unattached or misaligned chromosomes, thus, failure of the SAC machinery is a candidate mechanism involved in the generation of aneuploidy during mitosis (Fig. 4). It has been showed that deregulation of SAC components induces aneuploidy and tumor formation in cell culture and mouse models. Knockout of many spindle checkpoint genes, such as CENP-E, MAD2, BUB1, BUBR1 were shown to be embryonic lethal (Abrieu et al. 2000; Dobles et al. 2000). However, mice with impaired SAC survive and their cells can divide even though

the chromosomes are not aligned properly leading to aneuploid cells (Foijer et al. 2008; Li et al. 2009; Schvartzman et al. 2010).

MAD2 deregulation in the cells induces premature sister chromatids separation and aneuploidy (Meraldi et al. 2004; Lentini et al. 2012; Veneziano et al. 2016). Likewise, was found that MAD2 or BubR1 haploinsufficiency condition can induce aneuploidy and mitotic alterations in human primary fibroblasts and in near diploid colon cancer cells (Lentini et al. 2012; Lentini et al. 2014).

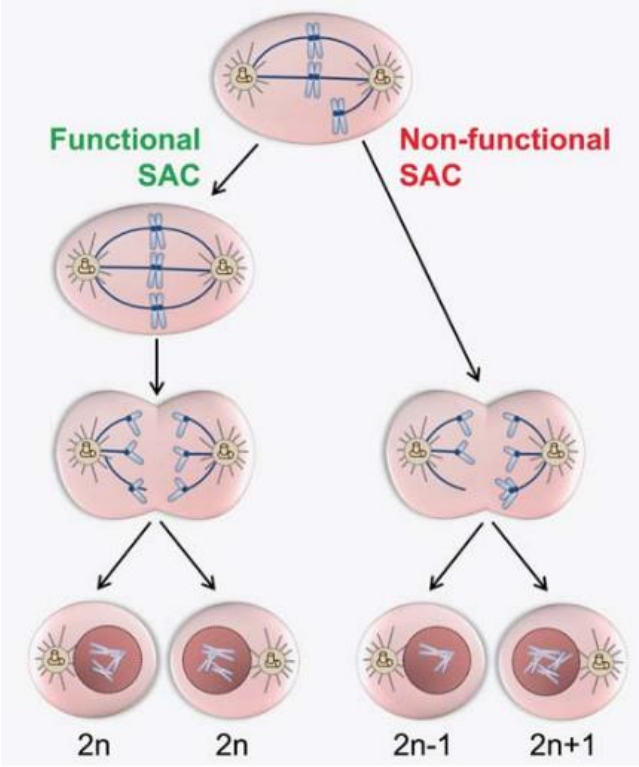

Fig 4: Generation of aneuploidy by non-functional SAC (Simonetti et al. 2019).

1.2 Centromere Associated Protein E

Chromosome congression is required for chromosome segregation and genomic stability during cell division (Barisic et al. 2014). Accurate chromosome segregation during mitosis requires the amphitelic attachment of kinetochore of duplicated chromosomes to spindle microtubules emanating from opposite poles (Cleveland et al. 2003). Microtubule capture

by the kinetochore is a stochastic process, consequently during the early stages of chromosome alignment, microtubules from one spindle pole temporarily may attach to either (monotelic attachment) or both sister kinetochores (syntelic attachment) (Fig. 5). undesirable attachments such as syntelic or merotelic attachments are usually corrected into amphitelic attachments before the onset of anaphase (Yamagishi et al. 2014; Cimini & Degrassi 2005). These improper kinetochore attachments, if not resolved, can lead to chromosome missegregation and aneuploidy (Holland & Cleveland 2009).

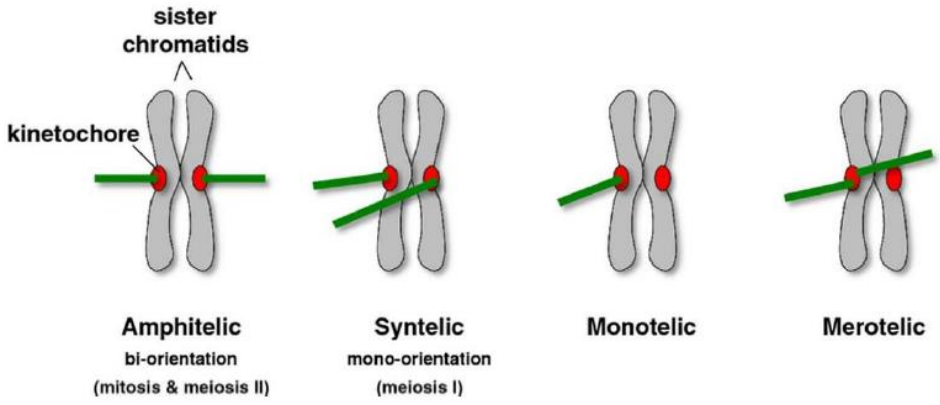

Fig. 5: Types of kinetochore–microtubule attachment (Yamagishi et al. 2014).

The kinetochore is a complex multiprotein structure consisting of structural and dynamic components, including centromere proteins (CENPs) that are required for microtubule capture and structural maintenance during chromosome alignment.

In this process an important role is mediated by CENP-E (Centromere Associated Protein-E), also called KIF10, a plus-end directed kinesin-7 motor protein of 316 kDa required for chromosome segregation in both mitosis and meiosis (Yen et al. 1992; Schaar et al. 1997; Kim et al. 2008). CENP-E protein contains a tail domain, a stalk domain and a motor domain (Fig. 6). CENP-E tail domain can mediate its diffusion on microtubules, the stalk domain is required to control physical interactions between CENP-E and spindle microtubules, but is not essential for its functions as a transporter and the motor domain is required for ATP hydrolysis and force generation (Gudimchuk et al., 2018).

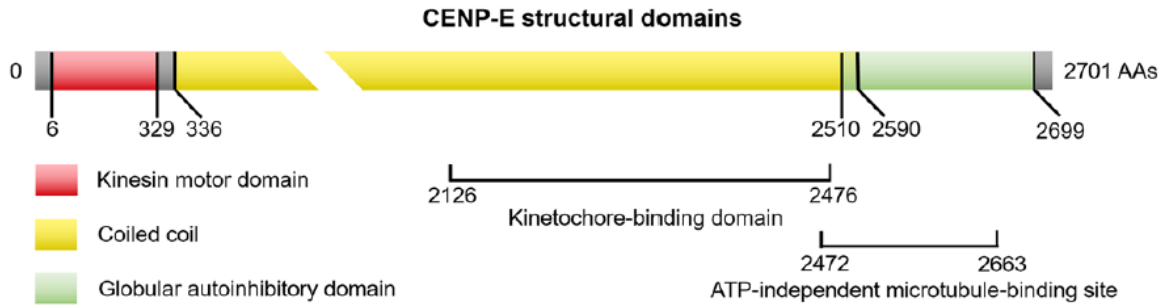

Fig. 6: Domain structures of human CENP-E protein (Yu et al. 2019).

CENP-E accumulates in late G2, functions during mitosis, and is degraded at the late stage of mitosis as quantitatively as cyclin B (Brown et al. 1994). Moreover, emerging evidence indicate that CENP-E is also precisely regulated by cell cycle regulators in the transcriptional level during cell cycle. Enhancer of rudimentary homolog (ERH), together with the spliceosome protein SNRPD3, regulates CENP-E's mRNA transcript splicing (Yu et al. 2019). During mitosis, CENP-E localizes to kinetochores, where it is one of a number of proteins that serve as linkers between chromosomes and the microtubules of the mitotic spindle (Gudimchuk et al. 2013). CENP-E interacts with spindle assembly checkpoint (SAC) components to prevent chromosome missegregation and aneuploidy (Abrieu et al. 2000; Weaver et al. 2003). CENP-E association with the kinetochore has been reported to be mediated by a large number of kinetochore-associated proteins with which it interacts, including the centromeric protein F (CENP-F), NUF2, and SKAP (Huang et al. 2012; Liu et al. 2007). Also CENP-E binds and, in the absence of bound microtubules, activates the SAC kinase BubR1 forming a stable ternary complex (spindle microtubule/CENP-E/BubR1) and producing checkpoint signaling that is silenced either by spindle microtubule capture or the tension developed at kinetochores (Mao et al. 2005).

It was reported that CENP-E can be multiply phosphorylated during mitosis (Nousiainen et al. 2006). However, the significance of all of these phosphorylations has not been established, but some of these can regulate CENP-E functions. Phosphorylation of the C-terminal tail of CENP-E by Cdk1, MAPK, or Mps1 has been proposed either to regulate CENP-E motor activity prior to its binding to kinetochores or inhibit a microtubule binding site in the tail (Espeut et al. 2008). Furthermore, it was discovered an Aurora/PP1 phosphorylation switch that is required not only for congression of polar chromosomes through modulation of the intrinsic motor properties of CENP-E, but also for subsequent

stable bi-orientation of those chromosomes (Kim et al. 2010). In the regulation of CENP-E, the Aurora kinase activity is opposed by Protein Phosphatase 1 (PP1) functions (Liu et al. 2010). It has been shown that PP1 can localize at outer of kinetochore and it can stabilize kinetochore-microtubule attachment by counteracting Aurora B kinase activity. In particular, Aurora kinases, both A and B, phosphorylate a single conserved residue close to the CENP-E motor domain while PP1 has a docking domain that overlaps the site of phosphorylation so the PP1 bind to CENP-E is disrupted by Aurora mediated phosphorylation. Aurora A phosphorylates CENP-E near the spindle poles, releasing PP1 from CENP-E. CENP-E phosphorylated is active and able to bind the microtubules to KMN network on the kinetochore thus to carry the chromosomes the spindle equator along the K-fiber of an already bi-oriented chromosome (Kapoor et al. 2006). As chromosomes congress, kinetochores move away from the Aurora A gradient concentrated at the spindle poles and CENP-E is dephosphorylated and recruits a high local concentration of PP1 to the outer kinetochores of chromosomes so it has translocated away from a pole. CENP-E delivered PP1 and dephosphorylation of kinetochore key components, such as Ndc80 and KNL1, is essential for stable kinetochore-microtubule interactions (Kim et al. 2010) (Fig. 7).

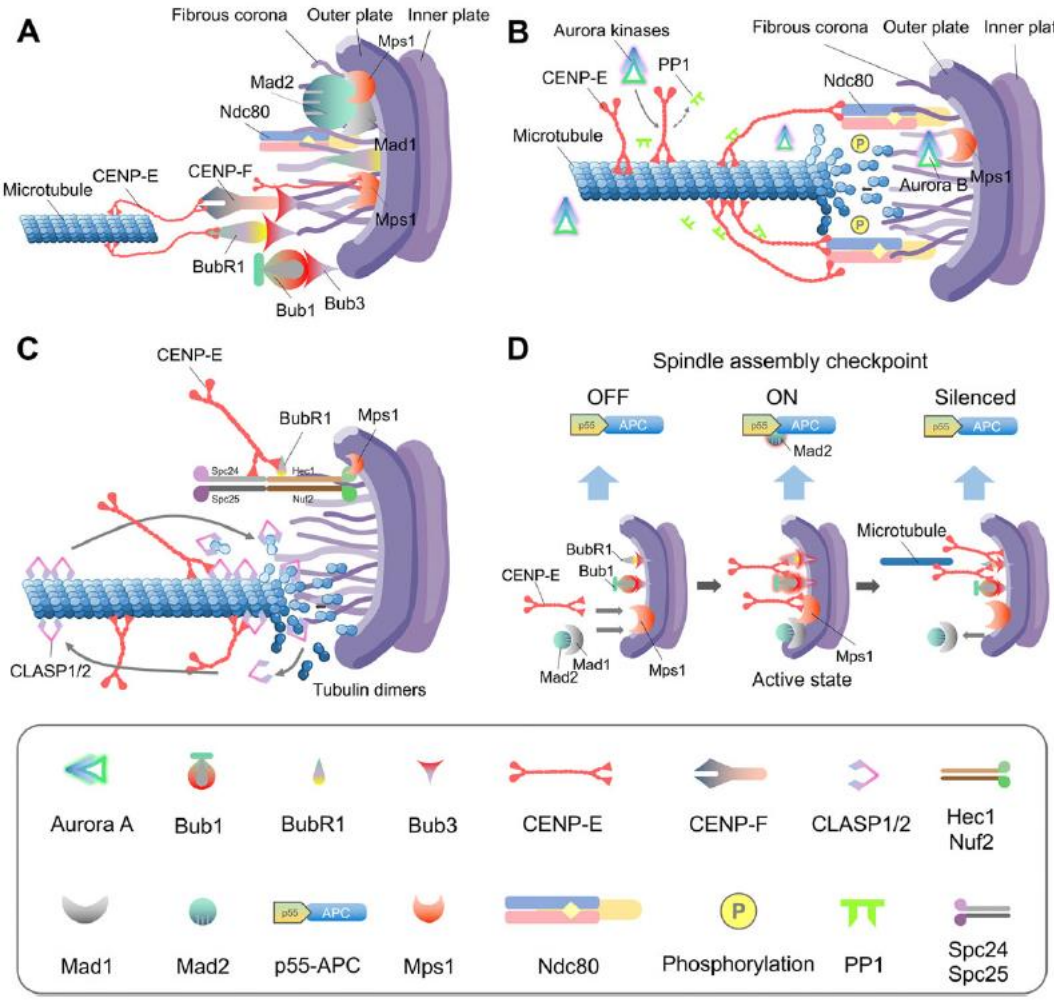

Figura 7: CENP-E partner proteins in cell division. CENP-E interacts with BubR1, CENP-F, Ndc80 complex (A), Aurora A/B kinases (B), CLASP1/2 (C). CENP-E and BubR1 interaction in Spindle assembly checkpoint (D) (Yu et al. 2019).

1.3 The specific inhibitor of CENP-E: GSK923295

Mitosis is a well-known target for chemotherapy, CENP-E is expressed during mitosis and plays critical roles in accurate chromosome alignment, thus CENP-E might represent a druggable target for several solid tumors that do not have targeted therapy (El-Arabey et al. 2018). GSK923295 is a highly selective anti-mitotic chemotherapy drug, and it interacts with CENP-E's motor domain. GSK923295 is an allosteric inhibitor, which specifically binds to the ATPase binding site of the CENP-E's motor domain (Balamuth et al., 2010) and non-competitively inhibits the ATPase activity of CENP-E with high selectivity (Wood et al., 2010) (Fig.8).

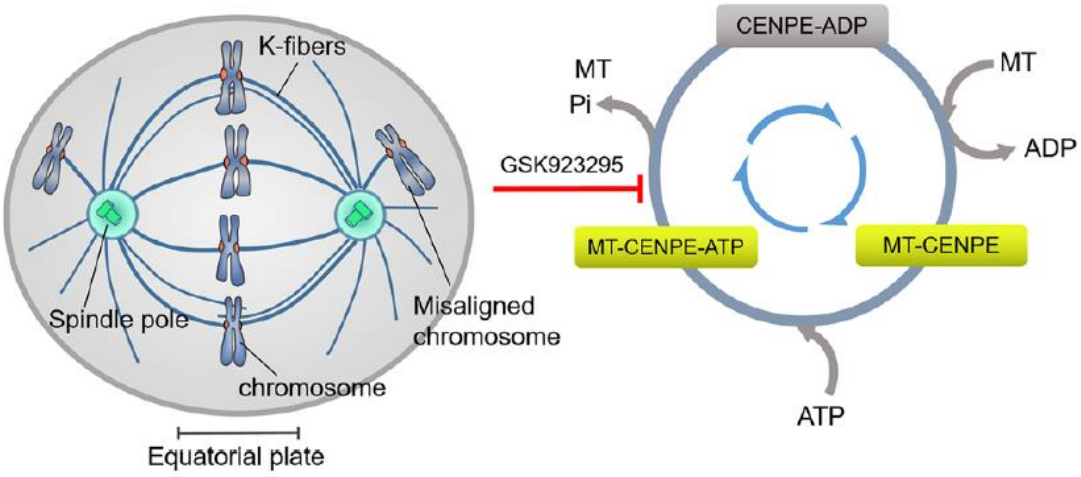

Fig. 8: GSK923295 mechanism of action (Yu et al. 2019).

GSK923295 treatment leads to the failure of metaphase chromosome alignment and induces mitosis arrest. In the presence of GSK923295, DLD-1 colon cancer cells show the majority of chromosomes aligned at metaphase, but few chromosomes remain close to the spindle poles. The kinetochores of these unaligned chromosomes stained for Bub1, indicating that the SAC is active and that kinetochore-microtubule attacks are not correct (Bennett et al. 2010).

1.4 The effects of aneuploidy on trascriptome and proteome

Aneuploid cells show large number of genes that are lacking or present in excess and this may lead to imbalances in production of mRNAs and proteins. Stochasticity of the event makes it difficult to predict which chromosome will be lost or gained, and therefore which genes result alterated in each aneuploid cell. Moreover it has been shown that aneuploidy does not only affect the expression of the genes located on the extra chromosomes, but also of multiple other genes across the entire genome (Torres et al, 2007; Sheltzer et al, 2012; Stingele et al, 2012). Despite the complexity of the stress to which they are subjected, aneuploid tumor cells must have acquired traits that allow them to tolerate the adverse effects of chromosomal imbalances and to proliferate. Omics studies showed that aneuploidy leads to common alterations in several pathways conserved between species

(Sheltzer et al, 2012). However, the same categories of pathways were consistently up or downregulated in different aneuploidies independently of the specific chromosomal aberration (Torres et al, 2007; Stingele et al, 2012; Dürrbaum et al, 2014).

Transcriptome and proteome analysis of trisomic MEFs (murine embryonic fibroblasts) and aneuploid human cells showed deregulation of DNA and RNA metabolisms, DNA repair, cell cycle progression, splicing and ribosome biogenesis and up-regulation of inflammatory and stress responses (Sheltzer et al, 2012; Stingele et al, 2012; Dürrbaum et al, 2014; Dephoure et al, 2014).

Despite the conserved pathway deregulation in different aneuploidies, the genes alterated inside these pathways are not shared between different aneuploidy models, this finding make it difficult to identify an aneuploidy gene signature, it seem that each cell line cope differently to aneuploidy stress, however with the same physiological response (Dürrbaum et al, 2014).

1.5 Aneuploidy vs. Tumor Suppressor pathways

As discussed above SAC weakening is sufficient to generate aneuploidy. However it has been demonstrated that aneuploidy have deleterious effects on cellular fitness in both yeast and mammalian cells (Torres et al. 2007; Siegel & Amon 2012). The aneuploidy induced by SAC gene alteration, in many case, generates a modest increase of tumorigenesis because the cell active control pathways to limit aneuploidy proliferation. For example, MAD2 depletion generate aneuploidy in primary human fibroblasts that active a senescence cellular pathway p53/p21-mediated (Lentini et al. 2012). This anti-proliferative effect can be mitigated by genetic alterations that allow cells to tolerate the adverse effects of aneuploidy, and by mutating genes that restrict proliferation of aneuploid cells, such as p53. Two of the most recurrent cytogenetic abnormalities observed among different types of cancers were gain of chromosome 8q (encoding the MYC oncogene) and loss of 17p (where is localized the TP53 tumor suppressor gene) suggesting that aneuploidy could underlie transformation by amplification of oncogenes or loss of tumor suppressors (Nicholson & Cimini 2013).

In support of this hypothesis, it was observed that aneuploidy caused by MAD1 or MAD2 depletion enhances tumorigenesis of cells with a genetic background $p53^{-/-}$ (Holland &

Cleveland 2009). However, loss of p53 allows highly aneuploid cells to proliferate in vitro (Li et al. 2010; Thompson & Compton 2010; Janssen et al. 2011), but does not directly cause euploid cells to become aneuploid (Bunz et al. 2002). At the same time, CENP-E heterozygous and p19/ARF null mice developed much more easily and with greater frequency spontaneous tumors compared to mice heterozygous for CENP-E but $p19^{ARF}$ wt (Weaver et al. 2007). Perhaps, loss of a tumor suppressor such as p53 is a prerequisite for the development of aneuploidy in human tumors, or an event required immediately after aneuploidy induction to promote tolerance to the aneuploid state.

However the relationship between aneuploidy, CIN and tumorigenesis is not so simple. It was proposed that a moderately elevated rate of CIN could potentially allow transformation while too much or too little CIN would have no effect or even inhibit the carcinogenesis process (Weaver & Cleveland 2007). Silk et al. showed that exacerbating the level of CIN in $CENP\text{-}E^{+/-}$ mice by crossing them to $MAD2^{+/-}$ or $p19^{ARF-/-}$ mice or by treating them with the chemical carcinogen DMBA resulted in enhanced cell death and reduced tumor incidence (Silk et al. 2013). A possible explanation of these observations is that eukaryotic cells have acquired surveillance mechanisms that actively prevent the propagation of highly aneuploid cells (Giam & Rancati 2015). In this case, while too much CIN could activate these protection mechanisms and target the cell to death or arrest, a moderate level of CIN might allow aberrant cells to keep proliferating. Accordingly, the tumor suppressor p53 is upregulated upon aneuploidization and has been shown to limit the proliferation of aneuploid cells in culture (Thompson & Compton 2010; Li et al. 2010; Lentini et al. 2012; Veneziano et al. 2016). A possible stress pathway that could play a role is the p38/p53 pathway that limits proliferation of aneuploid cells (Thompson & Compton 2010). Recently, alternative pathways were proposed to reduce proliferation of aneuploid cells through activation of $p14^{ARF}$/p53 apoptosis or cellular senescence p53/p21 mediated (Veneziano et al. 2016; Lentini et al. 2012). These results suggested that $p14^{ARF}$ could be a potential target that aneuploid cells use to overcome restriction mechanisms of cell proliferation. Further data showed that $p14^{ARF}$ is involved in the control of genomic stability in $p53^{-/-}$ cells; $p53^{-/-}$ MEFs and also $ARF^{-/-}$ MEFs and $ARF^{-/-}/p53^{-/-}$ double knockout MEFs had defects in chromosome segregations that were restored by $p14^{ARF}$ with the cooperation of Aurora B (Britigan et al. 2014).

In summary, CIN and aneuploidy have tumor-promoting abilities that are limited by anti-proliferative effects associated with aneuploidy. When these anti-proliferative effects are

suppressed through aneuploidy-tolerating mutations, such as tumor suppressor genes, the full tumorigenic potential of the condition is unleashed.

1.6 The tumor suppressor gene $p14^{ARF}$

The $p14^{ARF}$ protein is encoded by the INK4/ARF (CDKN2A) locus, one of the most commonly mutated or deleted in human cancers (Muniz et al, 2011; Sharpless et al. 1999). The same locus encodes another protein, $p16^{INK4a}$, also a potent inhibitor of cell proliferation. The mechanism by which these two proteins are produced is quite unusual: each transcript has a specific 5' exon, E1α or E1β for $p16^{INK4a}$ and $p14^{ARF}$ respectively, which are spliced to a common exon 2. This exon contains two overlapped ORFs, therefore the two proteins present amino acid sequences completely different (Fig. 9).

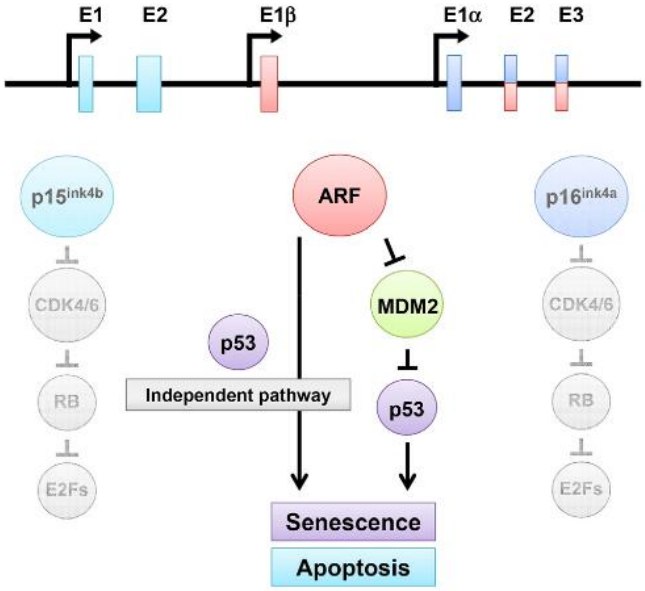

Fig. 9: The INK4A/ARF locus and tumor suppressor function of $p14^{ARF}$(Ko et al. 2018).

Under normal conditions, the $p14^{ARF}$ gene is repressed by the action of Polycomb proteins (PcG), which inhibit the expression of specific genes by chromatin modifications. BMI1 (B lymphoma Mo-MLV insertion region 1) is one of the main PcG components that repress $p14^{ARF}$ expression. In fact, murine embryonic fibroblasts (MEFs) BMI-1-/- show a detected upregulation of the expression of $p14^{ARF}$ and p16INK4a (Jacobs et al. 1999). The gene silencing PcG-mediated is also the molecular mechanism by which the p53 tumor

suppressor represses the $p14^{ARF}$ expression (negative feedback loop regulation). Indeed, p53 binds the promoter of $p14^{ARF}$ and recruits the complex histone deacetylation (HDAC) and PcG proteins (Zeng et al. 2011). $p14^{ARF}$ transcription is upregulated in response to a host of hyperproliferative signals including c-Myc, Ras, E2F-1, E1A, and v-Abl to induce cell cycle arrest (Sherr 2001).

INK4/ARF locus is frequently mutated or silenced in cancer cells. It has been reported that $p14^{ARF-/-}$ mice are highly cancer prone. Particularly, $p14^{ARF-/-}$ mice die after 1 year from spontaneous tumor development, with a mean survival latency of 38 weeks. Moreover, heterozygous mice also develop tumors after a longer latency than $p14^{ARF-/-}$ mice. The 43% of tumors observed in $p14^{ARF-/-}$ mice were sarcomas. In particular, a malignant osteogenic sarcoma with pulmonary metastasis and an agiogenic sarcoma metastatic to the liver were observed. The others tumors observed in $p14^{ARF-/-}$ mice were 29% of lymphomas, 17% of carcinomas and 11% of gliomas (Kamijo et al, 1999).

Although alterations of INK4a-ARF locus are not common in humans, they were found in roughly 30% of human tumors such as glioblastoma, melanoma, pancreatic adenocarcinoma (Maggi et al, 2014; Sharpless and DePinho, 1999; Sherr, 1998). In the majority of the cases all three proteins of the INK4b–ARF–INK4a locus are lost, making difficult to determine their individual roles in human tumor suppression. In particular, many mutations within exon 2 that affect both $p14^{ARF}$ and $p16^{Ink4a}$ are found in cancers (del Arroyo and Peters, 2005; Gardie et al, 1998; Rizos et al, 2001; Rutter et al, 2003; Zhang and Xiong, 1999). However, there are specific examples where only $p14^{ARF}$ appears to be affected in human cancer, and these cases appear to be most common in melanoma patients (Randerson-Moor et al, 2001). In addition to melanoma cases, nine of fifty glioblastoma patients have a specific deletion of $p14^{ARF}$ (Nakamura et al, 2001). Furthermore, the $p14^{ARF}$ promoter contains a CpG island, and $p14^{ARF}$ expression is frequently downregulated by promoter methylation (Maggi et al, 2014).

Taken together, this collective wealth of evidence clearly demonstrates the importance of $p14^{ARF}$ tumor suppression in human cancers. Because of the multiple roles played by $p14^{ARF}$ protein, it is conceivable to think that the alteration of its functions has a key role in the development of tumors.

1.7 p53-dependent $p14^{ARF}$ tumor suppression

One of the most well defined function of $p14^{ARF}$ protein is to suppress aberrant cell growth in response to oncogene insults by activating the transcription factor p53 that trigger the expression of many apoptosis inducers and cell cycle inhibitory genes (Ozenne et al. 2010). Among the many proteins counteracting genomic instability by ensuring genome surveillance and maintenance is the tumor suppressor p53 (Vousden & Lane 2007). p53 critically determines the fate of cells experiencing DNA damage, activating cell cycle arrest, senescence or apoptosis depending on the severity of the insult (Bieging et al. 2014). TP53 is mutated in approximately half of all human cancers and the frequently genetic alterations are missense mutations that disrupt p53's ability to act as a transcriptional activator (Kato et al. 2003; Junttila & Evan 2009). It is well known that p53, for its important role, is subjected to stringent multi-level regulation. It has been widely reported that the E3 ubiquitin ligase MDM2 (or HDM2) interacts with p53, blocks p53-mediated transactivation and, targets the p53 protein for rapid degradation (Chen et al. 1995; Kubbutat et al. 1997; Levine 1997). Furthermore, p53 itself stimulates the transcription of MDM2 binding its promoter, this determines the activation of a negative feedback system of p53 shutting down (Marine & Lozano 2010).

In presence of oncogenic stimuli $p14^{ARF}$ binds the C-terminal domain of MDM2 and keep it in the nucleolus where usually resides $p14^{ARF}$ because it has a specific amino acid sequence called NOLS. This event prevents the interaction between MDM2 and p53 and the transport in the cytoplasm of p53 and degradation MDM2-mediated (Pomerantz et al. 1998; Weber et al. 1999; Ozenne et al. 2010). By using deletion mutants of $p14^{ARF}$ protein (able or not to localize to the nucleolus) it has been shown that both binding to MDM2 and the localization of $p14^{ARF}$ protein in the nucleolus are necessary for $p14^{ARF}$-induced p53 stabilization, p53 activation and cell cycle arrest. In particular, the interaction between $p14^{ARF}$ and MDM2 sequestered MDM2 in the granular region of the nucleolus (Weber et al. 2000). Also $p14^{ARF}$ is able to inhibit the ARF-BP1/Mule protein, another E3 ubiquitin ligase that targets p53 (Chen et al. 2005).

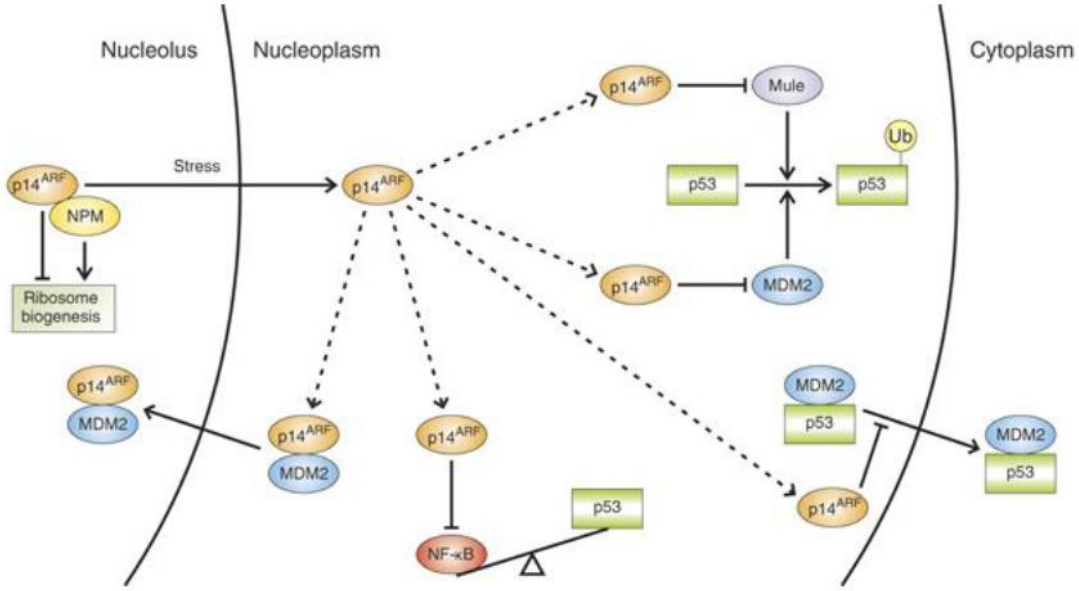

Figura 10: Schematic diagram of p53 stabilization and activation by p14ARF (Van Maerken et al. 2008).

In addition to the known function of MDM2 regulation by $p14^{ARF}$, a recent study describes a new mechanism through which MDM2 can in turn regulate $p14^{ARF}$ levels during the tumorigenic process. It was shown that MDM2 overexpression in various cancer cell lines causes $p14^{ARF}$ reduction inducing its degradation through the proteasome thanks to $p14^{ARF}$ phosphorylation PKC-mediated (Vivo et al. 2015).

1.8 p53-indipendent function of $p14^{ARF}$

Although $p14^{ARF}$ is undoubtedly a critical component of the p53 pathway, there are some evidences that $p14^{ARF}$ has also the ability to restrain cell growth independently of p53. Mice lacking ARF, p53 and MDM2 are more tumor prone compared to those lacking only p53 and MDM2. Furthermore, $ARF^{-/-}$ and $ARF^{+/-}$ mice develop a broader spectrum of tumors than p53-null mice (Weber et al. 2000). In line with this Weber and colleagues (2000) showed that ARF overexpression can induces a G1 arrest in cells lacking p53. In particular, in cells deficient for ARF/p53/MDM2 (derived from triple knockout or TKO mice), they observed that the reintroduction of wild type ARF was able to prevent S phase entry and/or trigger apoptosis by mechanisms that did not require the expression of wild-type p53 protein. They also demonstrated a significant reduction of colony formation in ARF infected TKO mice. Moreover, it has also been reported that $p14^{ARF}$ induces cell

cycle arrest in a p53-independent manner in human lung tumor cells (Eymin et al. 2003). In particular, $p14^{ARF}$ expression determined a G2 arrest followed by apoptosis both in ‘‘in vitro’’ and ‘‘in vivo’’ models. In this latter case, upon $p14^{ARF}$ overexpression a decrease of tumor growth and induction of lung tumors regression was observed in xenograft models.

Other studies support the idea that $p14^{ARF}$ also stimulates important pathways to maintain the genomics integrity and stability. In fact, in response to DNA damage caused by ionizing radiation, UV and genotoxic treatments, $p14^{ARF}$ intervenes either through a p53-dependent and p53-indipedent pathways. Together with p53, activated by kinases and ATR, it can induce cell cycle arrest and possibly apoptosis. However, it was seen that the activation of ATM/ATR signaling cascade may be upstream triggered from $p14^{ARF}$ protein that stabilizes the Tip60 protein, a histone acetyltransferase that activates ATM by acetylation (Eymin et al. 2006). Taken together these results support a role of $p14^{ARF}$ in mediating p53- independent tumor suppressive functions and suggest that $p14^{ARF}$ also acts independently of the MDM2-p53 axis in tumor surveillance.

In line with this, it has been reported that $p14^{ARF}$ can interacts with a multitude of different cellular partners: proteins involved in transcriptional control (E2Fs, DP1, p63, c-Myc, Hif1α), nucleolar proteins such as nucleophosmin (NPM/B23), viral proteins (HIV-1Tat), mitochondrial protein (p32) and many others (Sherr 2006). The variety of the $p14^{ARF}$ interactors strongly suggested that $p14^{ARF}$ has a wider role to protect the cell upon different types of insults. For example $p14^{ARF}$ interacts and antagonizes the transcriptional functions of Myc and E2F1, powerful oncogenes required for cell cycle progression, inducing their capture in the nucleolus or preventing the recruitment of their transcriptional coactivators (Eymin et al. 2001). Instead, other $p14^{ARF}$ partners like B23/NPM are degraded by the proteasome in an ubiquitin-dependent manner or few others like Tip60 or TOPO I become activated or stabilized (Pollice et al. 2008).

In addition, it has been described that $p14^{ARF}$ is able to promote sumoylation of some of its interactors. This modification can affects an high variety of phenomena such as protein stability, transport, modulation of gene expression (up-regulation or down-regulation), ubiquitination, DNA repair, and centromeric chromatid cohesion (Tago et al. 2005; Ozenne et al. 2010). In particular, it has been reported that $p14^{ARF}$ interacts with the Myc-associated zinc finger protein Miz1 and, by inducing its sumoylation, facilitates the assembly of the Myc-Miz1 complex that cause the switch from G1 arrest to apoptosis (Herkert et al. 2010). It has been shown that $p14^{ARF}$ can induce sumoylation of both

MDM2 and nucleophosmin NPM/B23 (Maggi et al. 2014). Although the precise mechanism underlying this $p14^{ARF}$ function is currently unknown it has been suggested that it explicates this function through a direct interaction with the sumo-conjugating enzyme Ubc9. Additionally, $p14^{ARF}$ also inhibits the function of a de-sumoylating protein, SENP3 (Haindl et al. 2008). Although $p14^{ARF}$ involvement in the sumoylation process is well documented, the biological meaning of $p14^{ARF}$ mediated sumoylation is still unclear.

As $p14^{ARF}$ is mainly localized in the nucleolus this led to the hypothesis that it might play a role in the ribosomal biogenesis (Saporita et al. 2007). In fact, there are data that show inhibition of rRNA processing following the downregulation of NPM mRNA. In addition, it has been shown by blocking NPM nucleo-cytoplasmic shuttling that $p14^{ARF}$ is able to interfere with the ribosome export resulting in a delayed rRNA transcription and processing (Itahana et al. 2003; Sherr 2006).

AIM OF RESEARCH

In this study, I wanted to investigate the mechanisms that determine the promotion and tolerance of aneuploidy in human cells.In the first part of my PhD I focused my attention on the relationship between aneuploidy induced by SAC gene weakening, and tumor suppressor genes, in particular I investigate the role of $p14^{ARF}$ tumor suppressor gene in counteracting aneuploidy induced by partial depletion or inhibition of the mitotic kinesin CENP-E, required for faithfully chromosomes segregation.

To this aim I used post-transcriptional silencing of CENP-E, which works only in the SAC signalling, to induce aneuploidy in HCT116 cells and in IMR90 cells to investigate the involvement of $p14^{ARF}$ on aneuploid cell proliferations. Then, I induced $p14^{ARF}$ expression ectopically in HCT116 cells, in which $p14^{ARF}$ is not functional because of the presence of an allele with a mutation and the other with the promoter hypermethylated (Burri et al. 2001). I generate HCT116 cells expressing a functional $p14^{ARF}$ by two different systems: a retroviral inducible (Tet-OFF) vector pBPSTR1 and a piggyBac transposon inducible (Tet-ON) system. I evaluated the level of aneuploidy and mitotic alterations in cells expressing or not $p14^{ARF}$ and the possible pathways (cellular senescence or apoptosis) activated by $p14^{ARF}$ to limit aneuploidy.

In the second part of my PhD I focused my studies in search of a possible molecular signature underlying aneuploidy and its toleration in human cells. To this aim I induced the post-transcriptional silencing, in human cells, of the CENP-E gene that if deregulated induces aneuploidy, and I analyzed whole genome expression using a DNA microarray approach.

CENP-E depletion in IMR90 primary human fibroblasts induced aneuploidy that was maintained for two weeks. To identify aneuploidy tolerance associated genes it was used a cDNA microarray approach, and I analysed the global gene expression profiles of early (72 hours post-RNAi) and late (2 weeks post-RNAi) aneuploid IMR90 cells induced by CENP-E depletion.

Finally, I identified by different bioinformatics tools genes and pathways significantly deregulated in these samples.

RESULTS

2.The tumor suppressor p14^{ARF} counteract aneuploid cells proliferation

2.1 CENP-E knockdown by RNA-Interference induces aneuploidy

To investigate the role of p14^{ARF} in response to aneuploidy and the fate of aneuploid cells, I induced aneuploidy in human cell lines by partial depletion of centromere-associated protein-E (CENP-E) using RNA interference, mimicking CENP-E haploinsufficiency. To ascertain if partial depletion of CENP-E induced aneuploidy in IMR90 primary human fibroblasts and HCT116 cells, I transfected cells with two CENP-E specific siRNAs (siCENP-E#1, siCENP-E#2) and with an unspecific siRNA targeting the green fluorescent protein (siGFP) as a control. I performed a RT-qPCR (Fig. 11A-B) and a Western Blot (Fig. 11C-D-E) to quantify siRNAs effects at transcriptional and protein levels. CENP-E reduction that mimicks haploinsufficiency RNAi was obtained by using the siCENP-E#1 in HCT116 cells and the siCENP-E#2 in IMR90 cells.

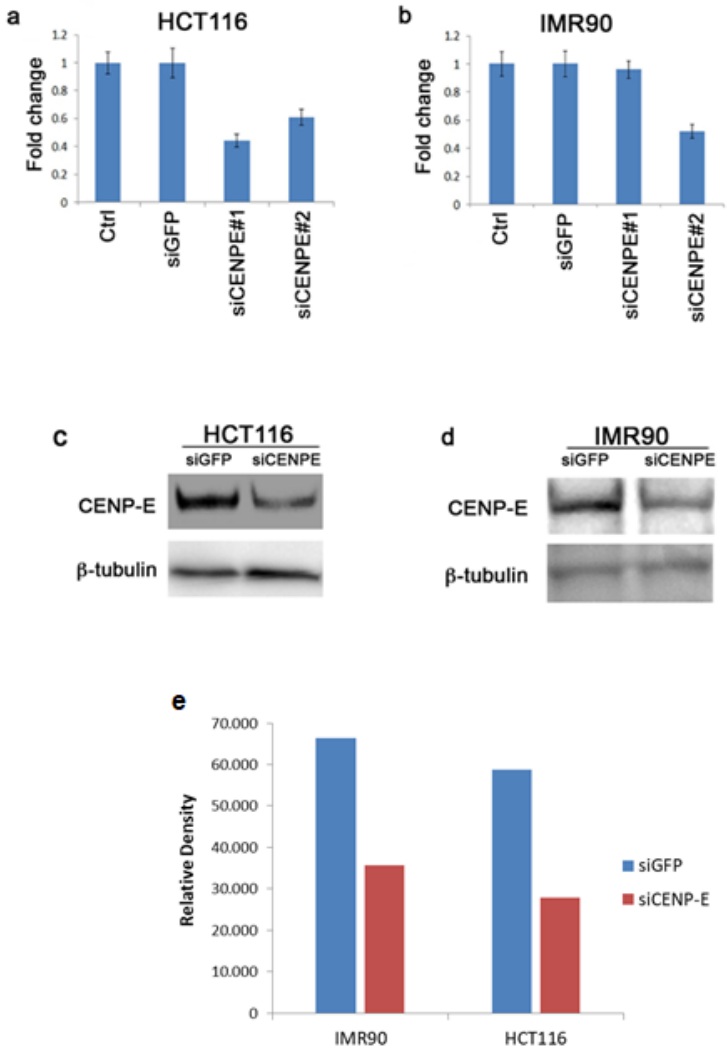

Fig. 111: RT-qPCR (a-b) and Western Blot (c-d) show decreased levels of CENP-E transcript and protein in transfected HCT116 and IMR90 cells, demonstrating the efficacy of post-transcriptional silencing by both siRNAs. (e) Quantification using ImageJ, densitometric data was normalized with respect to β-tubulin.

In addition, immunofluorescence experiments to visualize the CENP-E amount at the single cell level in siGFP (control) and siCENP-E cells, confirmed a 50% reduction of the CENP-E signal in both IMR90 and HCT116 siCENP-E pro-metaphase cells (Fig.12a-b).

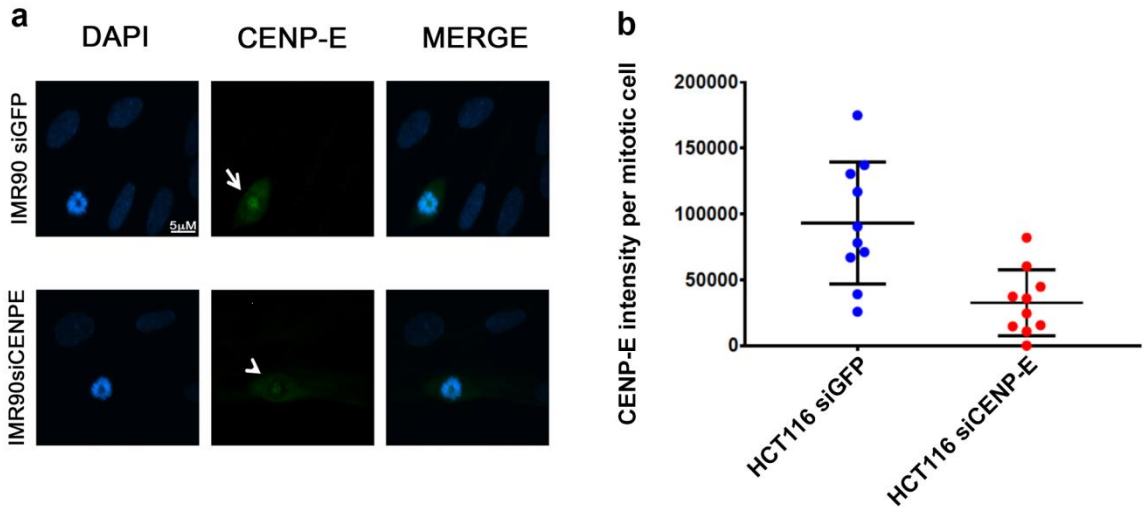

Fig. 112: Immunofluorescence assay. On the right representative images of CENP-E partial knockdown in IMR90 detected by CENP-E antibody (DNA was stained with DAPI); on the left Box plot confirming partial knockdown in HCT116 cells.

To assess whether CENP-E partial depletion affected cell proliferation I evaluated the cellular density per dish at 24, 48, and 72 h post-transfection. While there was no statistically significant difference in proliferation of HCT116 siCENP-E cells compared to control cells (Fig. 13 a), the IMR90 cells transfected with the siRNA targeting CENP-E showed a reduced proliferation at 24 h compared to the control cells (Fig.13 b).

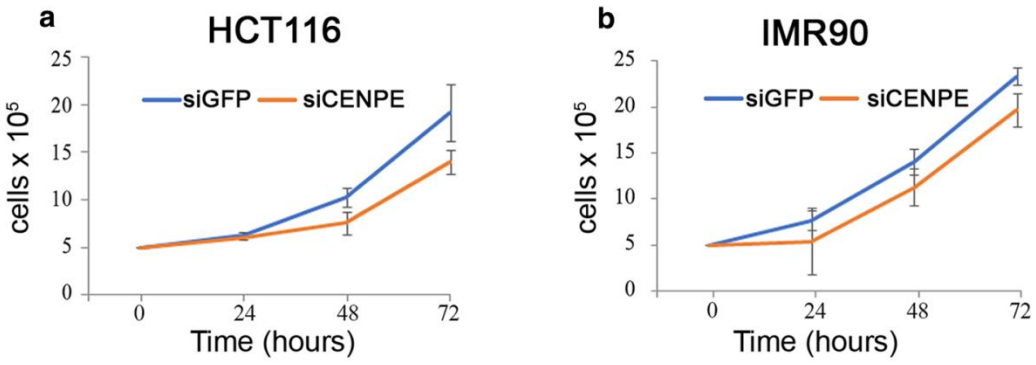

Fig. 113: Graph showing HCT116 and IMR90 cell proliferation after transfection with siRNA targeting CENP-E in respect to siGFP control cells.

However, at 48 and 72 h IMR90-siCENPE and IMR90-siGFP cells showed a similar cell number, and cell cycle analysis by cytofluorimetry showed that CENP-E partial depletion does not stop the mitotic progression of IMR90 cells (Fig15). Thus, CENP-E partial depletion

does not seem to affect the proliferation of IMR90 and HCT116 cells. Furthermore, I analysed cytofluorimetric profiles by the Modfit software and this analysis showed the presence of a remarkable percentage of aneuploid cells in IMR90 siCENP-E cells (49%) respect to control cells (0%).

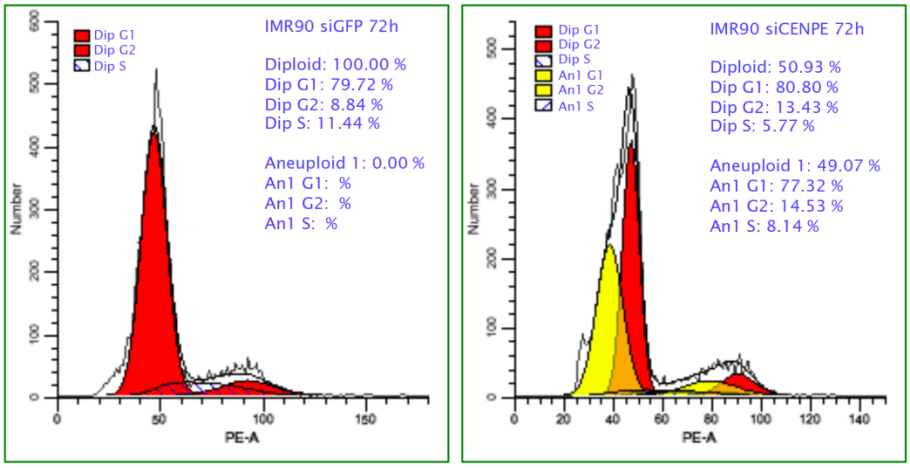

Fig. 114: Cytofluorimetric assay with PI stain to compare cell cycle profile of IMR90 cells transfected with siCENP-E respect to control cells. Cytofluorimetric profiles were analyzed with ModFit software.

To assess if weakening the SAC by CENP-E partial depletion induces aneuploidy in IMR90 and HCT116 cells, as previously shown in MEFs (Weaver et al. 2007), I analysed IMR90 and HCT116 cells transfected with siCENP-E by cytogenetics. Indeed, CENP-E post-transcriptional silencing in both cell lines resulted in significantly more aneuploid cells than control cells. Interestingly the percentage of aneuploid cells is higher in HCT116 cells lacking of functional expression of $p14^{ARF}$ tumor suppressor, than that showed by IMR90 cells (Fig. 15).

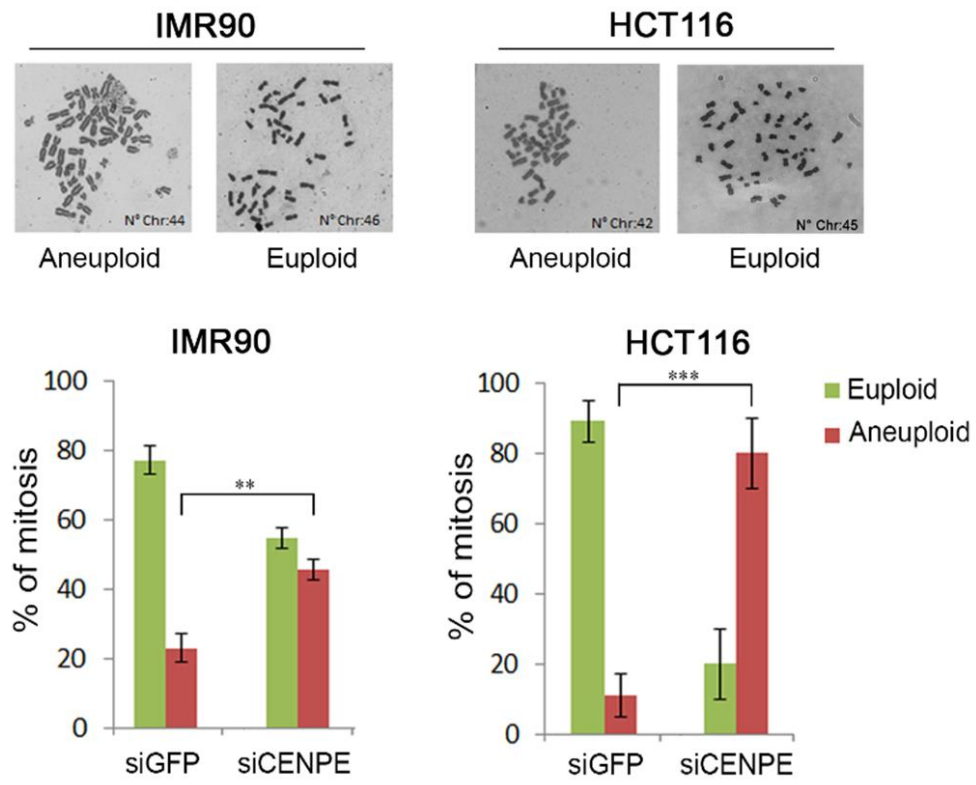

Figura 115: Representative pictures of aneuploid and euploid metaphases observed in IMR90 and HCT116 cells. The graphs below the pictures show the relative percentages of euploid and aneuploid cells.

2.2 Aneuploidy is maintained at longer time in cells lacking p14^{ARF} expression

It is known that incorrect karyotype reduces the proliferative capacity of cells (Sheltzer and Amon 2011). Therefore, I evaluate the differences in proliferation rates between aneuploid cells generated by CENP-E partial depletion in IMR90, HCT116 cells and control cells (siGFP). Cells were analyzed by metaphase spreads up to 4 weeks after siRNA transfection (72 hours, 2 and 4 weeks time points). Fifty percent of IMR90-siCENP-E cells remained aneuploid up to 2 weeks compared to 20% scored in IMR90-siGFP cells (control). However, 4 weeks after CENP-E depletion the percentage of aneuploid cells in IMR90 siCENP-E dropped to 22.5%. HCT116-siCENP-E cells showed 80% and 48% of aneuploid cells after 72 hours and 2 weeks, respectively. Four weeks after RNAi treatment, HCT116-siCENP-E cultures still showed 40% aneuploid cells, a percentage which is higher than that observed in IMR90 siCENP-E cells at the same time point (Fig.16).

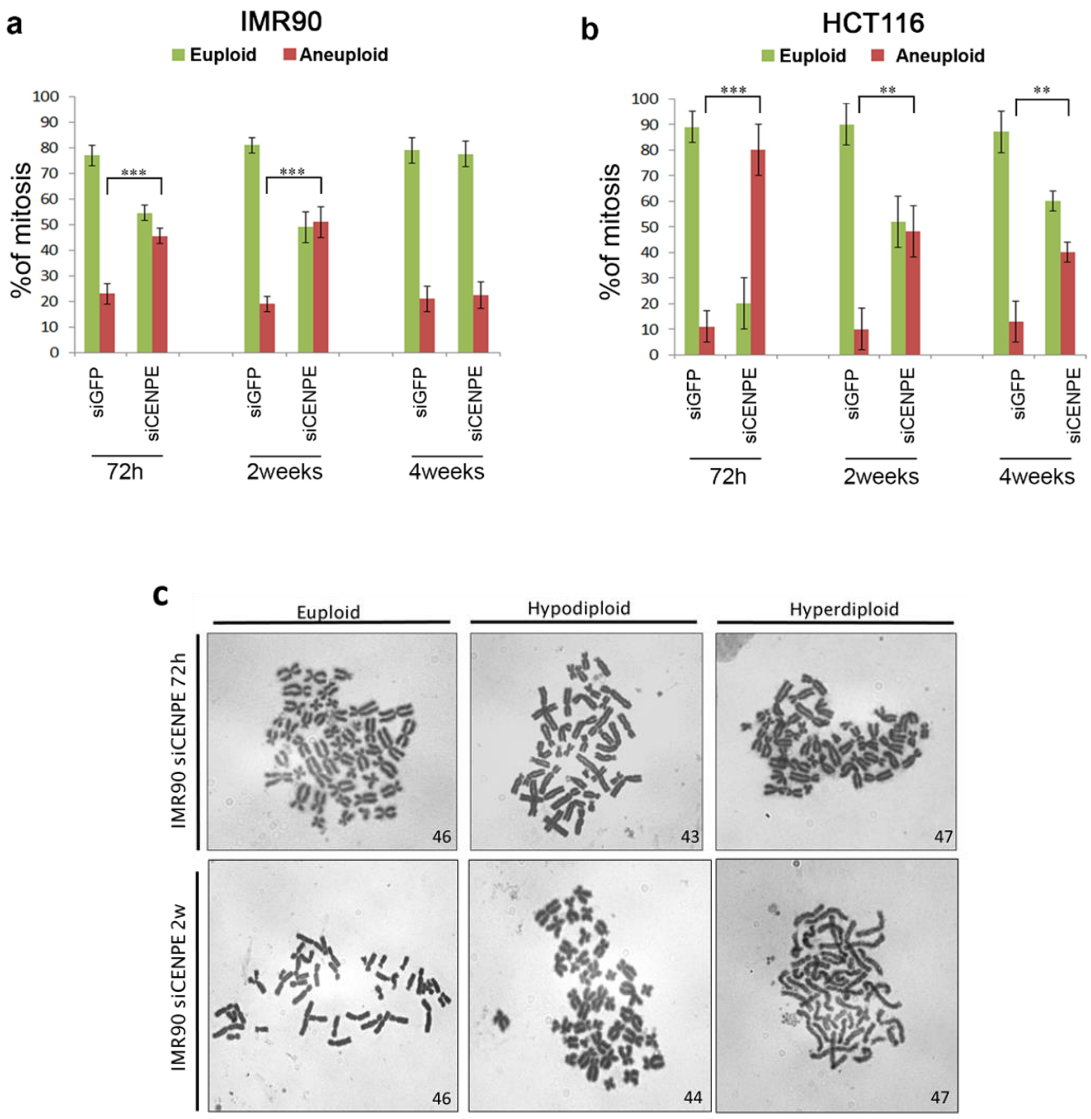

Fig. 116: Cytogenetic analysis shows aneuploidy reduction in IMR90 cells (a) and not in HCT116 cells (b). c) Pictures showing GIEMSA stained euploid, hypodiploid and hyperdiploid representative metaphases in CENP-E depleted IMR90 cells at 72h and 2 weeks after transfection.

Recently, it has been showed that $p14^{ARF}$ ectopic expression reduced the number of HCT116 aneuploid cells in cultures depleted for MAD2, suggesting a role for $p14^{ARF}$ in controlling proliferation of aneuploid cells (Veneziano et al. 2016). Based on this observation, we hypothesize that the reduction of aneuploid cells in CENP-E partially depleted IMR90 cultures over time might be caused by an increased expression level of $p14^{ARF}$. To explore this hypothesis, I measured the $p14^{ARF}$ gene expression levels in IMR90 siCENP-E cells over time. I observed, that at 72 h post-siCENP-E transfection, the $p14^{ARF}$ mRNA level in IMR90 siCENP-E cells were similar to the level observed in control cells (IMR90 siGFP). However, at 2 and 4 weeks after CENP-E knockdown $p14^{ARF}$ gene expression levels increased (Fig.17).

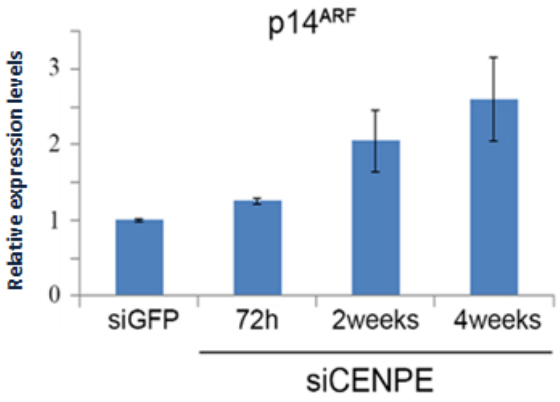

Fig. 17 RT-qPCR showing $p14^{ARF}$ transcript levels in IMR90 siCENP-E cells at 72 hours, 2 weeks and 4 weeks after transfection compared to control (siGFP).

2.3 $p14^{ARF}$ counteracts aneuploidy induced by CENP-E partial depletion

It has been reported that $p19^{ARF}$ knockout MEFs displayed a combination of mitotic defects and aneuploidy (Britigan et al. 2014). To verify if this occurs also in human cells $p14^{ARF}$ depleted we used RNAi in aneuploid IMR90-siCENP-E cells. Consistently with our hypothesis, I found that double-depleted CENP-E/$p14^{ARF}$ IMR90 cells displayed an increased fraction of aneuploid cells (78%) compared to IMR90 cells depleted of either $p14^{ARF}$ or CENP-E (aneuploid fractions 52% and 57%, respectively) (Fig.18). This result strongly suggests the involvement of $p14^{ARF}$ in the aneuploidy control.

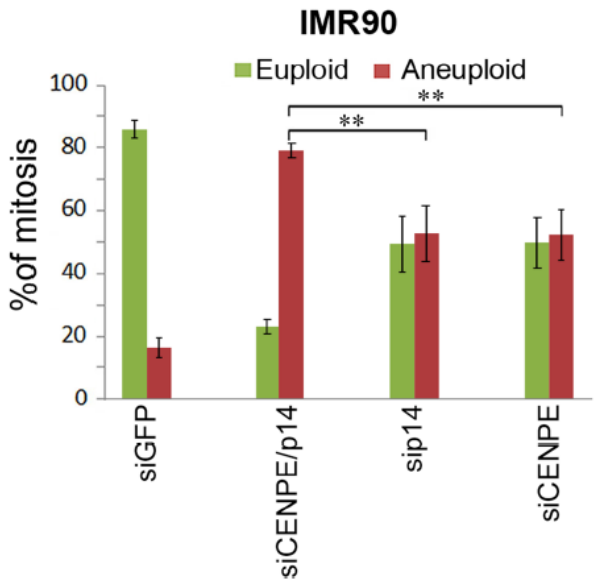

Fig. 117: Cytogenetic assay shows that simultaneous depletion of CENP-E and $p14^{ARF}$ produced an effect almost additive on aneuploidy in IMR90 cells.

To evaluate if different p14^{ARF} expression levels may modulate the effect induced by CENP-E depletion in the cells, I engineered a tetracycline-regulated (Tet-off) retroviral vector (pBPSTR1) (Veneziano et al. 2019) for the inducible expression of p14^{ARF} to be transfected in nearly diploid HCT116 tumor cells lacking a functional p14^{ARF} (Burri et al. 2001).

RT-qPCR and immunofluorescence analyses confirmed an increased level of p14^{ARF} transcript and protein in pBPSTR1-p14^{ARF} HCT116 cells when compared to cells transduced with a pBPSTR1-H2BGFP control vector and wild type HCT116 cells (WT) (Fig. 19).

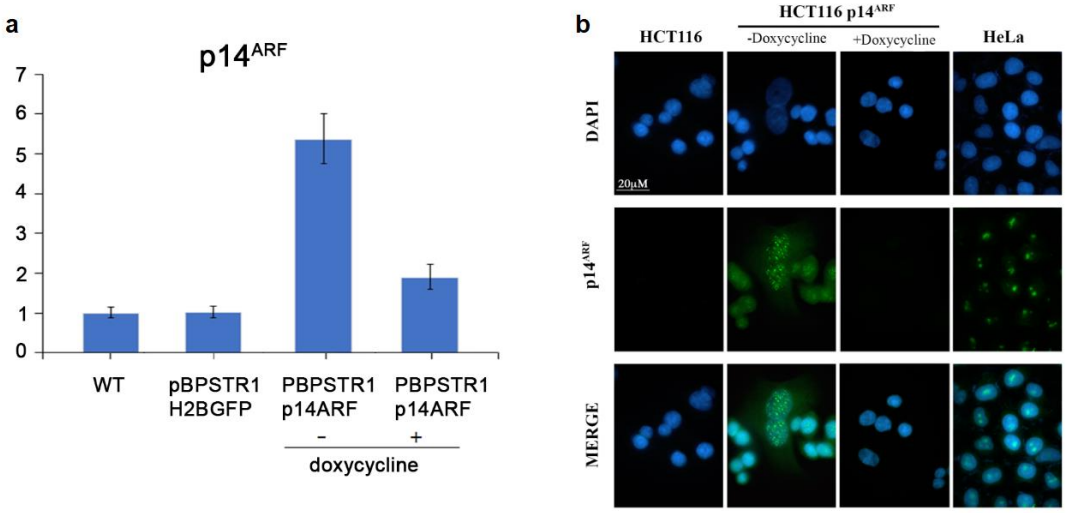

Fig. 118: RT-qPCR (a) and Immunofluorescence assay (b) showing p14^{ARF} transcript levels in HCT116 pBPSTR1 cells. Doxycycline treatment turns off p14^{ARF} expression.

To confirm the hypothesis that p14^{ARF} tumor suppressor gene has an important role in limiting the proliferation of aneuploidy cells I combined p14^{ARF} re-expression with CENP-E partial depletion. The presence of p14^{ARF} drastically reduced the percentage of aneuploid cells from 80% in siCENP-E HCT116 cells to 22% in siCENP-E HCT116 cells expressing p14^{ARF} .(Fig.20)

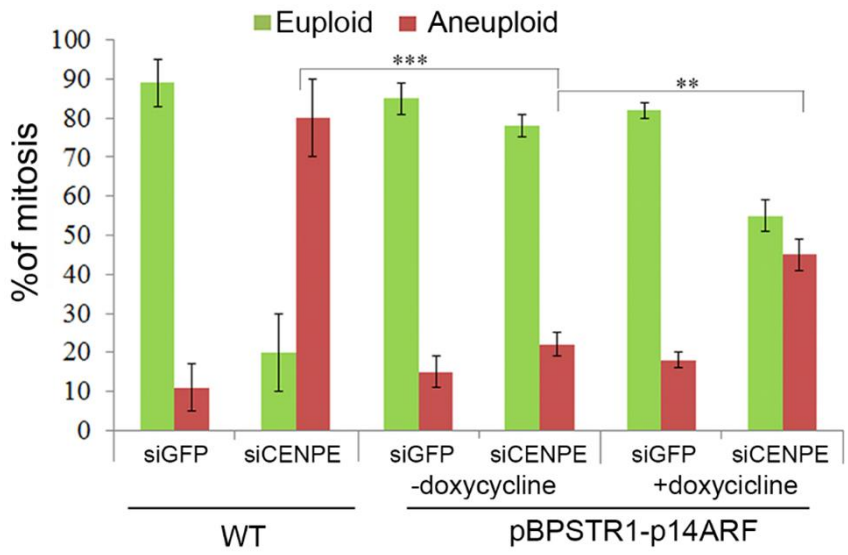

Fig. 2019: Cytogenetic analysis showed that when combined with CENP-E partial depletion, $p14^{ARF}$ expression drastically reduced the percentage of aneuploid cells.

Importantly, HCT116 cells that expressed ectopic $p14^{ARF}$ did no longer show defects in mitotic progression after CENP-E partial depletion or doxycycline treatment (Fig.21)

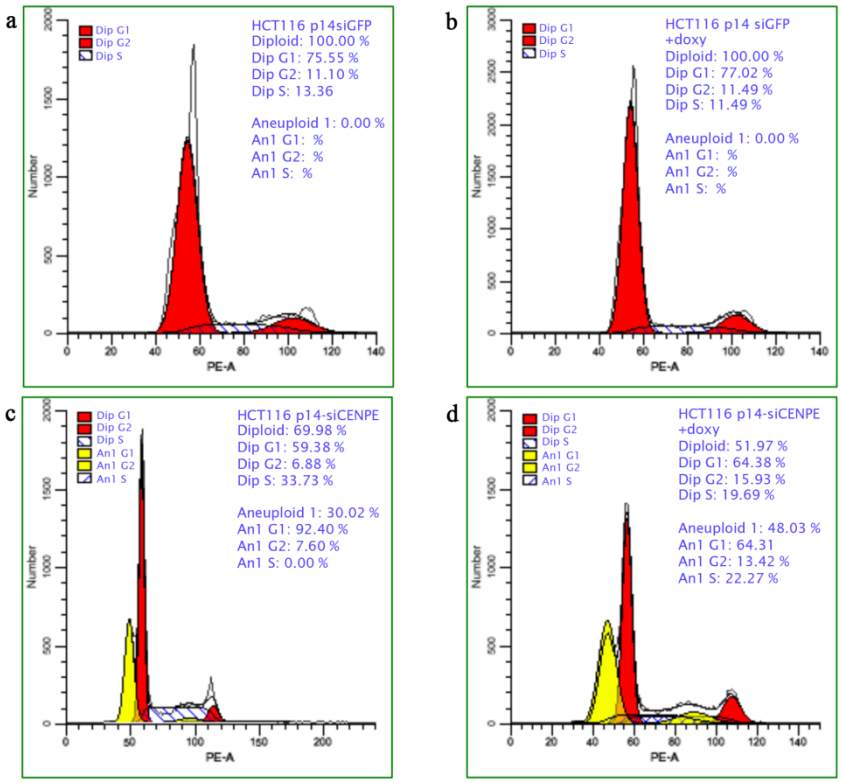

Fig.21: Cytofluorimetric assay with PI stain to compare cell cycle profile of HCT116 pBPSTR1 cells transfected with siCENP-E respect to control cells. Cytofluorimetric profiles were analyzed with ModFit software.

These results suggest that cells with reduced expression of $p14^{ARF}$ cannot properly counteract aneuploidy confirming and extending the crucial role played by $p14^{ARF}$ in the maintenance of genomic stability.

2.4 p14^{ARF} counteracts aneuploidy induced by CENP-E inhibition by GSK923295

Previous results suggest that cells lacking of the tumor suppressor p14^{ARF} respond differently to the induction of aneuploidy. It is known that genetic background plays a key role in the control of aneuploidy generation. For example, alteration of CENP-E gene induces aneuploidy in MEFs and the simultaneous absence of ARF significantly increases its levels. In addition it was shown that MEFs ARF$^{-/-}$ become aneuploid suggesting a role of the p14^{ARF} tumor suppressor in the control of aneuploidy (Silk et al. 2013). Moreover, the observation that depletion of SAC genes (MAD2 and CENP-E) induces aneuploidy which is increased in human cells lacking of p14^{ARF} expression, suggests that p14^{ARF} plays a role in limiting aneuploidy (Veneziano et al 2016).

To further evaluate if different p14^{ARF} expression levels may modulate the aneugenic effects caused by CENP-E inhibition, I cloned the p14^{ARF} cDNA into a tetracycline-regulated (Tet-ON) PiggyBac Transposon Vector (ePB) for its inducible expression of p14^{ARF} in nearly diploid HCT116 cells (Fig.22).

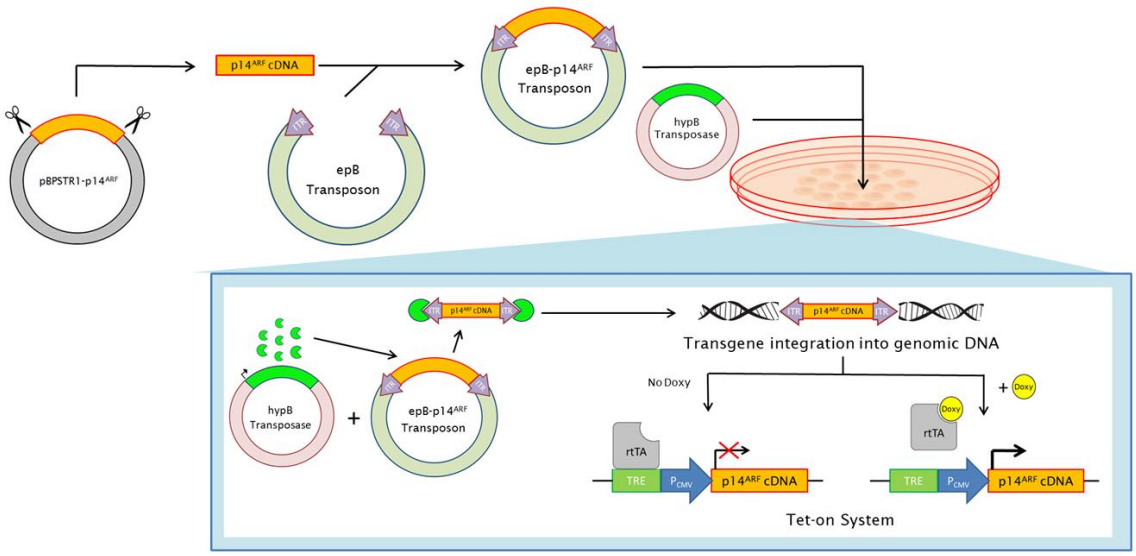

Fig.22: Experiment design scheme

2.4.1 Cloning of p14^{ARF} c-DNA into the PiggyBac vector

The PiggyBac transposon is a mobile genetic element that efficiently transposes between vectors and chromosomes via a "cut and paste" mechanism. During transposition, the PiggyBac transposase recognizes transposon-specific inverted terminal repeat sequences (ITRs) located on both ends of the transposon vector and moves the contents from the original sites and integrates them into TTAA chromosomal sites (Wilson et al. 2007).

The p14^{ARF} c-DNA was isolated from pBPSTR1 retroviral vector where it was cloned in the PmeI restriction site. To assure the correct extraction of the p14^{ARF} insert the restriction enzymes BamHI and NotI cutting upstream and downstream of the insertion site were used (Fig.23). Gel electrophoresis confirmed the extraction of the full-length c-DNA as revealed by the ≈ 500bp band (Fig.23). The c-DNA was then purified from the agarose gel for cloning in the ePB vector. The ePB vector was digested with BamHI e NotI to generate compatible sticky ends, and gel electrophoresis confirmed the linearized ePB vector (6250bp). The ePB vector was then, dephosphorylated with alkaline phosphatase to prevent its circularization in the next step of ligation.

The ligation mix (ratio of 1:5 plasmid/insert) was used to transform E. coli competent cells. To verify the presence of the ePB -p14^{ARF} construct the positive colonies were analyzed by the PCR colony assay with primers matching inside of the p14^{ARF} c-DNA (Fig.23). Six bacterial colonies containing the ePB -p14^{ARF} construct (Fig 24) were detected and plasmid DNA was extracted from one of these colonies (Colony 1).

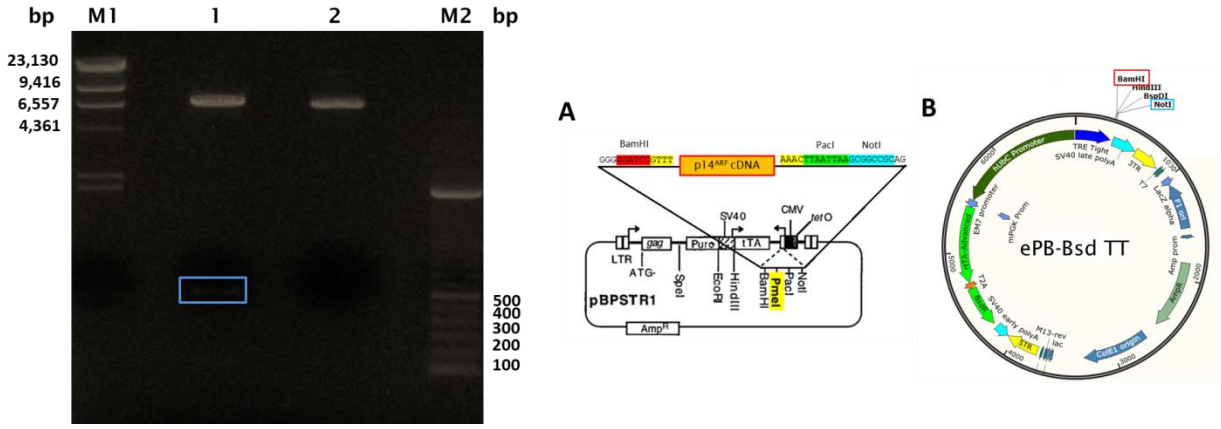

Fig. 2320: Gel electrophoresis. pBPSTR1-p14^{ARF} (A) and PiggyBac (ePB)(B) vectors were digested with BamHI (Lane1) and NotI restriction enzymes (lane 2). The blue box shows the fragment containing the p14^{ARF} cDNA. The fragment was then purified from the gel and ligated in ePB vector. M1: ʎ HindIII marker; M2: 100bp ladder.

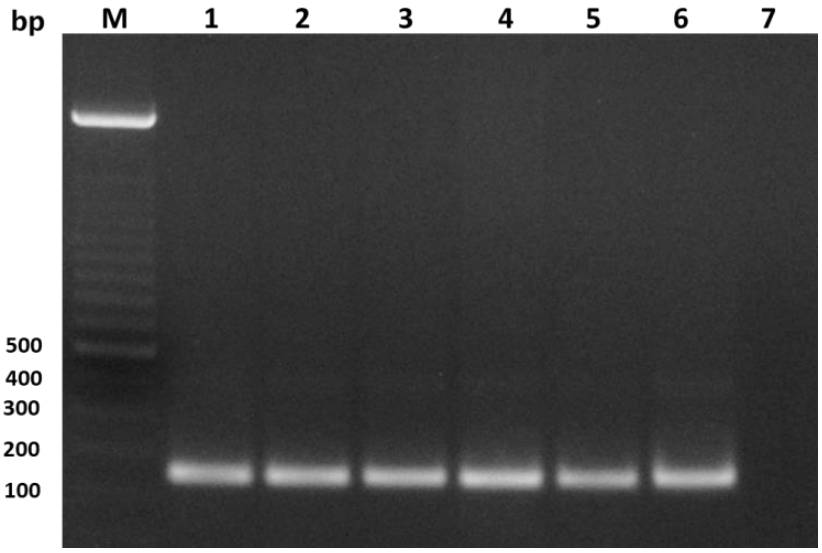

Fig.24: Colony PCR to detect ePB vector containing the p14 ^{ARF} cDNA. Competent E. coli TOP10 strain was transformed with ePB-p14^{ARF} vector and selected with ampicillin. Colony PCR with specific primers for the p14 cDNA showed that all the analyzed colonies were positive for the correct construction. Lane1-5: colonies #1-5; Lane6: purified pBPSTR1-p14 (positive control); Lane 7: no template. M: 100bp ladder

To verify the correct insertion/orientation of the p14^{ARF} c-DNA cloned into the plasmid, I performed a restriction analysis. The plasmid DNA extracted by the colony 1 was digested with BamHI and NotI that has a single cutting sites in the ePB vector in order to discriminate the correct length of the fragments obtained (Fig.). The plasmid DNA of the colony 1 was sequenced (BMR Genomics, Padua, Italy). The DNA sequencing confirmed the presence of the insert (Fig.25).

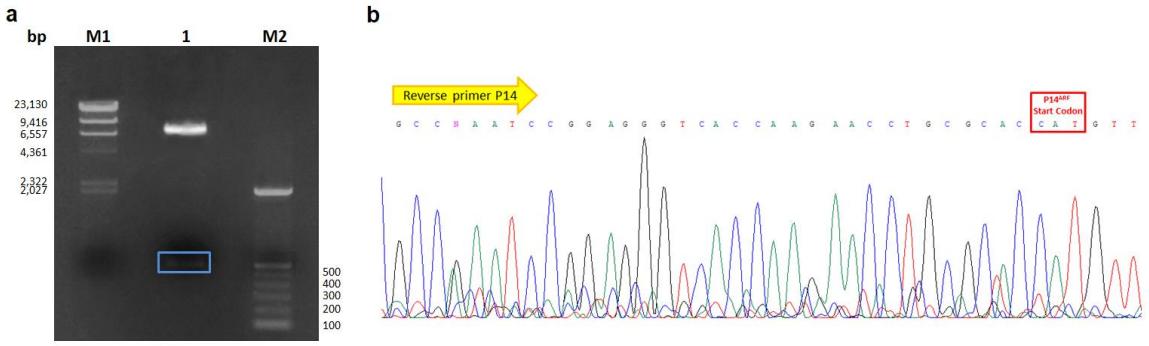

Fig. 2521: A) Restriction analysis of the ePB-P14^{ARF} vector. Double digestion of DNA extracted from colony #1 with BamHI and NotI restriction enzymes. The blue box indicates the p14^{ARF} cDNA containing fragment. M1: λ HindIII marker; M2: 100bp ladder. B) ePB-P14^{ARF} sequencing. Electropherogram of ePB-p14^{ARF} sequenced with a specific primer for p14^{ARF} cDNA. The red box indicates the p14ARF start codon.

2.4.2 Characterization of HCT116 cells expressing ectopic p14^{ARF}

To express ectopically p14^{ARF}, HCT116 cells were co-transfected with the ePB vector carrying the p14^{ARF} c-DNA and the vector carrying the trasposase (hyPB). Transfected HCT116 cells were then selected using Blasticidin (40µg/ml) for at least ten days.

To evaluate both the presence of the ectopic p14^{ARF} and the amount of its transcript level, I performed a genomic PCR reaction with specific primers mapping in the p14^{ARF} c-DNA sequence in stably transfected HCT116 cells. Agarose gel electrophoresis confirmed the presence of the p14^{ARF} insert in HCT116 ePB-p14^{ARF} cells after its amplification from genomic DNA (Fig.26.

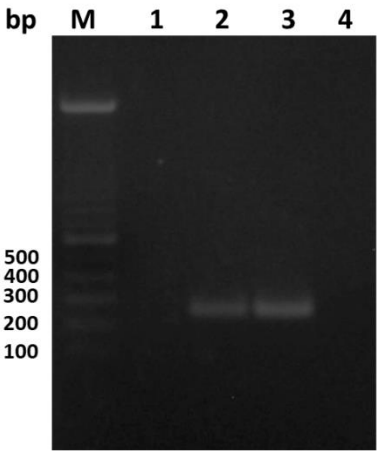

Fig.26: PCR of Genomic DNA to evaluate transgene integration. Lane1: HCT116 ePB empty vector (EV); Lane2: HCT116 ePB-p14^{ARF}; Lane3: ePB-p14^{ARF} (positive control); Lane4: no template.

I tested different doxycycline concentrations to assess the inducibility of the system. Initially, I tested a concentration of 2μg/ml for 24 hours. The RT-qPCR analysis showed that after the doxycycline treatment the levels of p14^{ARF} are highest in HCT116 ePB-p14^{ARF} cells compared to wild type HCT116 and to HCT116 cells harboring the empty ePB vector (Fig.27a). Moreover, immunofluorescence analysis showed the presence of the ectopic protein expressed induced by the treatment (Fig.27b). I evaluated the effects of p14^{ARF} re-expression on cell vitality and cell cycle progression. Proliferation assay showed a drastic decline in cell growth in HCT116 ePB-p14^{ARF} as well as in HCT116 cells carrying the empty vector (control). The cytofluorimetry analysis showed a partial block in the G1 phase in both samples after doxycycline treatment. This result suggests a detrimental effect of this concentration of doxycycline in these cells (Fig.27c-d). I treated then cells with reduced doxycycline concentration to optimize a concentration that allows correct re-expression of p14^{ARF} without toxic effects. I tested different doxycycline concentration: 1μg/ml, 500ng/ml, 250ng/ml, 125ng/ml, 30ng/ml (Fig.) and 10ng/ml. All these concentration of doxycycline, except 10ng/ml, turned out to have negative effects on cells (Fig.).

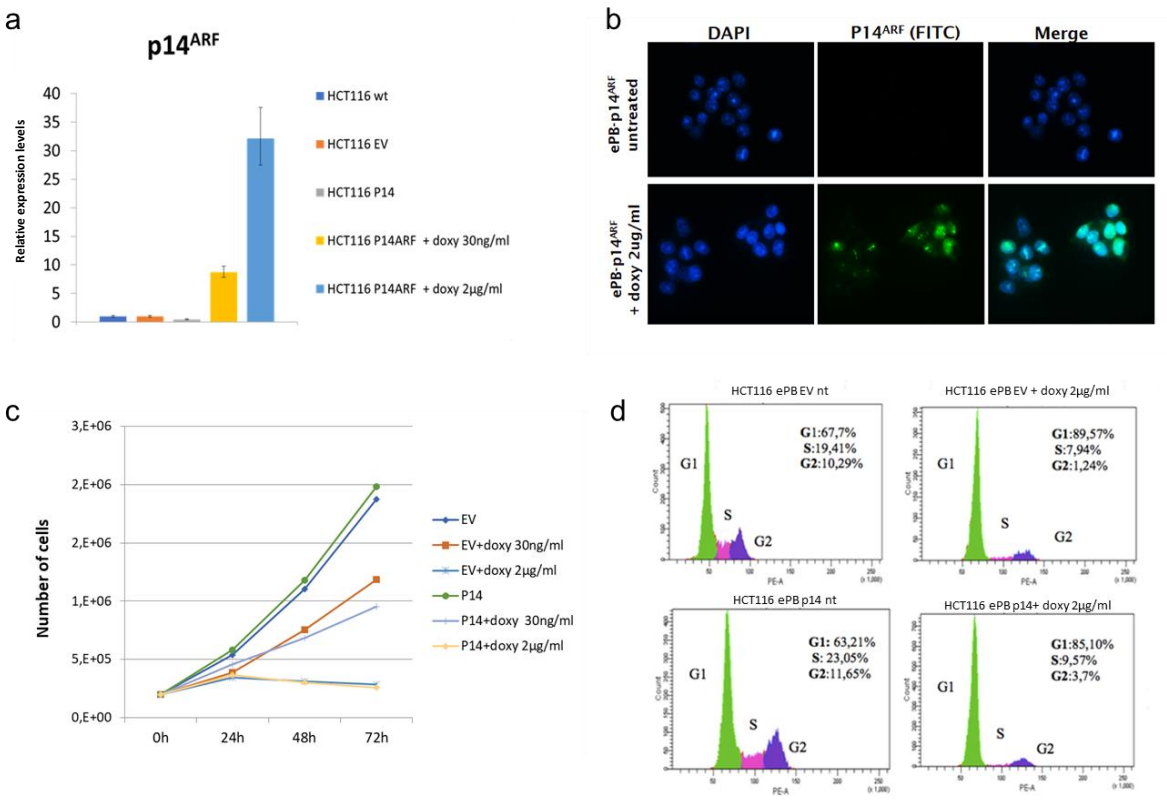

Fig. 2722: . HCT116 ePB-p14ARF cells show increased p14ARF transcript and protein levels after Doxycycline treatment. Untreated and doxycycline-treated HCT116 cells were analyzed by real time RT-PCR using specific primers for p14ARF (a) and by Immunofluorescence with a specific antibody against p14ARF (b). (c) Effects of p14ARF restoration on HCT116 cells proliferation. Growth curves of ePB–EV and ePB–p14ARF cells in absence and presence of Doxycycline 30ng/ml and 2µg/ml, respectively. (d) Cell cycle profile show a partial block in G1 phase following doxycycline treatment

Conversely, treatment with 10ng/ml of doxycycline did not affect cell proliferation and cell cycle profile in both HCT116 ePB empty vector and HCT116 ePB-P14^{ARF} cells. Furthermore, RT-qPCR and immunofluoresce p14^{ARF} showed transcript and protein levels higher than those present in control untreated (Fig.28).

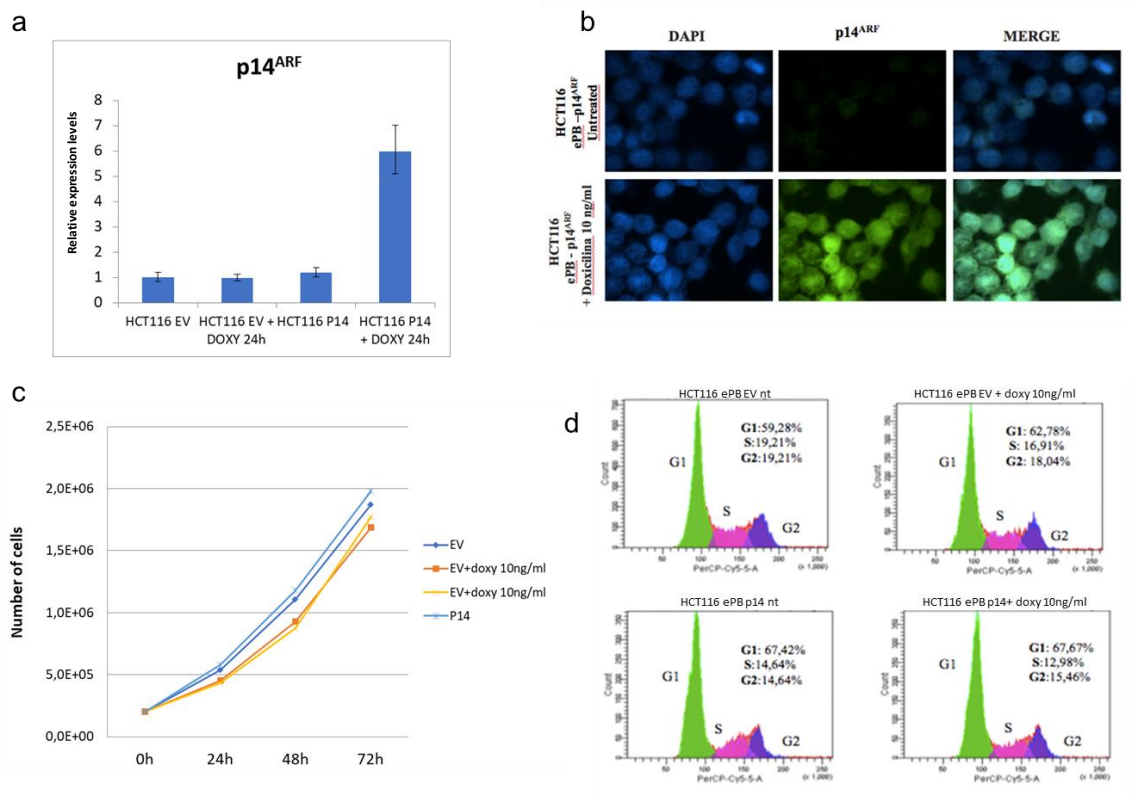

Fig. 2823: Characterization of HCT116 ePB-P14^{ARF} after 10ng/ml doxycycline treatment.

Moreover, Western Blot analysis confirmed that after 24 hours of exposure doxycycline induced p14^{ARF} protein expression in trasfected cells (Fig. 29)

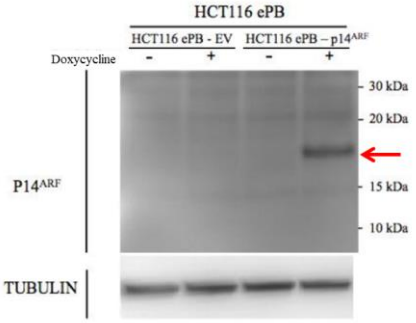

Fig. 2924: Western blot analysis confirmed p14^{ARF} protein increase 24h after dox treatment in HCT116 ePB-p14^{ARF}.

2.4.3 p14^{ARF} block proliferation of aneuploid cells induced by CENP-E inhibition

The small molecule GSK923295 is a specific inhibitor of the CENP-E kinesin. GSK923295 exposure allows most chromosomes to align at the cell equator but blocking a small number near the spindle poles. To test if CENP-E inhibition by GSK923295 induced aneuploidy in HCT116 near-diploid cells, I treated cells for 72 hours with GSK923295 at the concentration of 5nM, corresponding to IC50 that mimics CENP-E haploinsufficiency. Metaphase spread analysis showed a large increase in the percentage of aneuploid cells (65%) in GSK923295 treated cells in comparison to the untreated cells (18%).

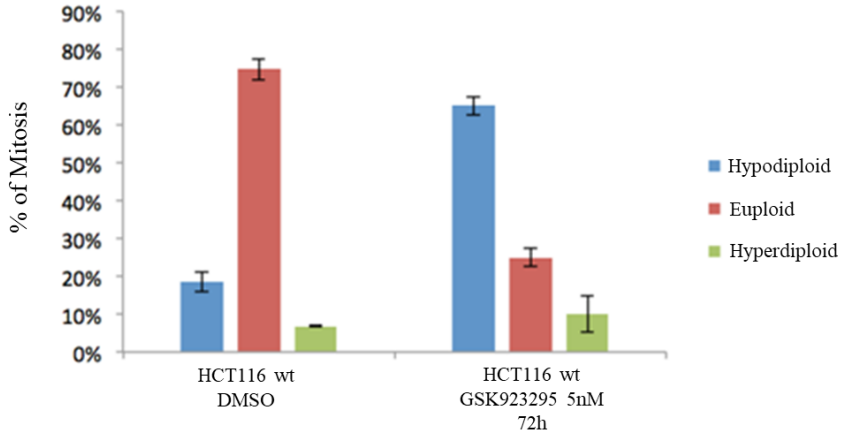

Fig. 3025: The graph shows the percentage of aneuploid HCT116 cells at 72 hours after treatment with GSK923295 5nM in respect to untreated cells (DMSO).

To evaluate if $p14^{ARF}$ re-expression rescues euploid phenotype in cells lacking $p14^{ARF}$, I treated HCT116 ePB-$p14^{ARF}$ cells with GSK923295 5nM for 72h to induce aneuploidy. Twenty hours before the end of the treatment $p14^{ARF}$ expression was induced by doxycycline (10ng/ml) and plody was analysed by metaphase spread. I used HCT116 cells transfected with the empty vector (HCT116 ePB EV) as negative control (Fig. 31a).

Cytogenetic assay shows that $p14^{ARF}$ re-expression greatly reduces the percentage of aneuploid cells induced by CENP-E inhibition. Following CENP-E inhibition, I found 65% of HCT116 ePB-p14 untreated cells hypodiploid compared to 18,5% in HCT116 ePB-p14 control cells (DMSO). After doxycycline treatment and $p14^{ARF}$ re-expression the percentage of hypodiploid cells dropped to 24%, as similarly observed in control cells (Fig.31 b). This result confirms that $p14^{ARF}$ could play a role in counteracting proliferation of aneuploid cells.

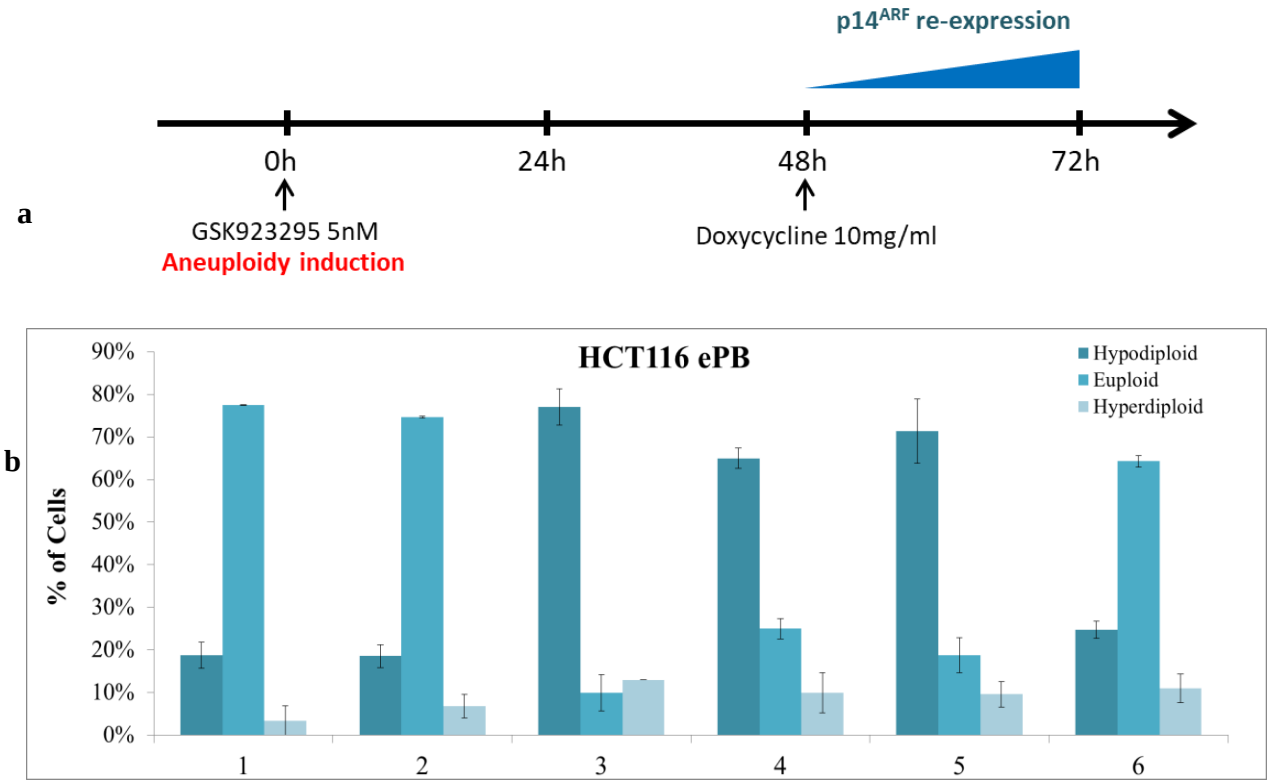

Fig.31: Graphs showing the results of the cytogenetic assay on HCT116 cells after 72h from treatment with GSK923295 5nM. (1) HCT116 ePB EV DMSO, (2) HCT116 ePB EV GSK923295, (3) HCT116 ePB EV GSK923295 + Dox, (4) HCT116 ePB p14 DMSO, (5) HCT116 ePB p14 GSK923295, (6) HCT116 ePB p14 GSK923295 + Dox.

To establish whether the reduced number of aneuploid cells induced by $p14^{ARF}$ re-expression was due to a cell cycle block, I performed a cell cycle profile analysis by cytofluorimetry with Propidium Iodide stain on HCT116 ePB-$p14^{ARF}$ and HCT116 ePB EV cells (Fig.32)

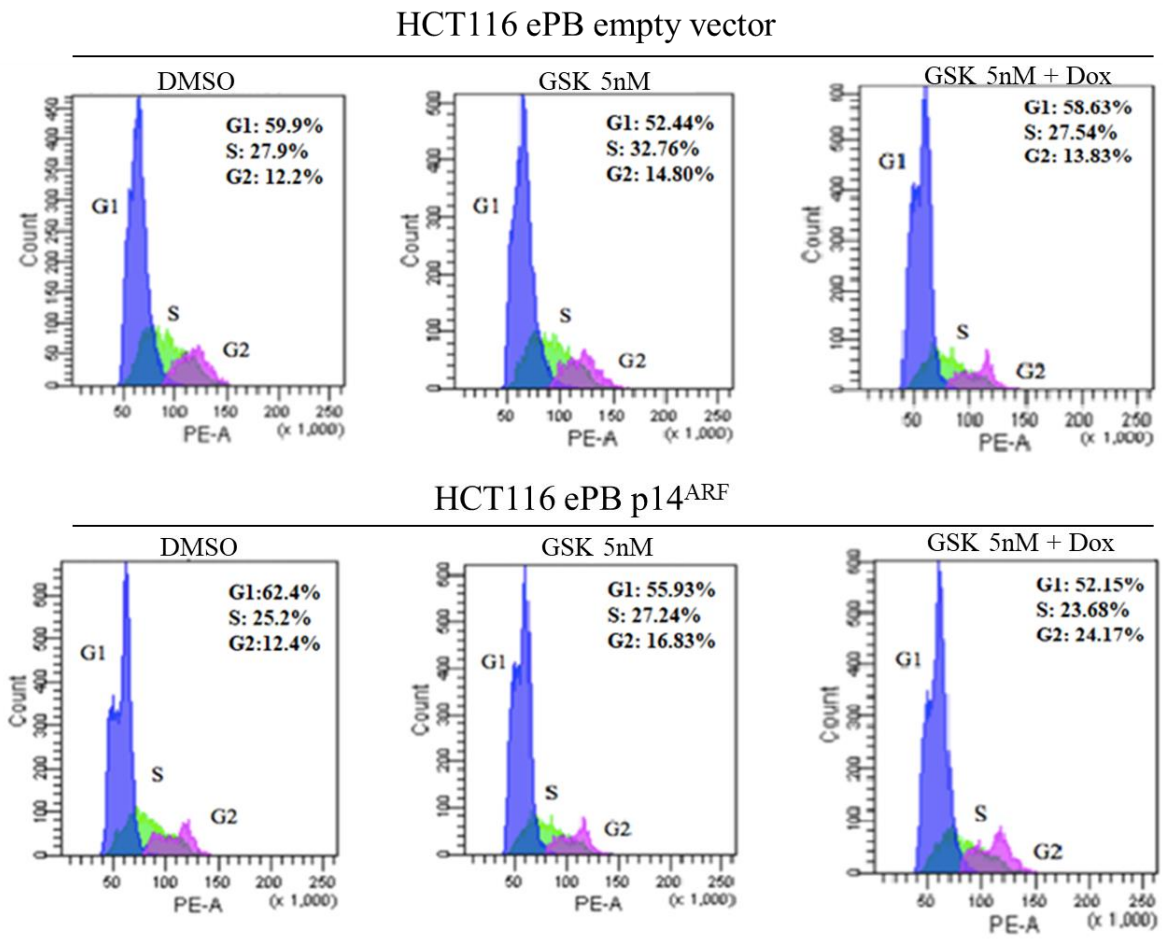

Fig. 32: $p14^{ARF}$ does not induce cells cycle alteration in GSK923295 treated cells. Cytofluorimetric profiles of HCT116 transfected with the empty vector (top) and with the vector expressing $p14^{ARF}$ (bottom).

I investigated whether p14^{ARF} could activate the senescence pathway after CENP-E inhibition in HCT116 cells. To this aim I conducted a senescence-associated β-galactosidase activity assay to evaluate the percentages of senescent cells after p14^{ARF} ectopic expression in GSK923295 treated cells. I found a low number of β-gal positive cells in all samples analyzed (Fig.33), suggesting that in aneuploid induced HCT116 cells ectopic expression of p14^{ARF} does not activate a cellular senescence pathway.

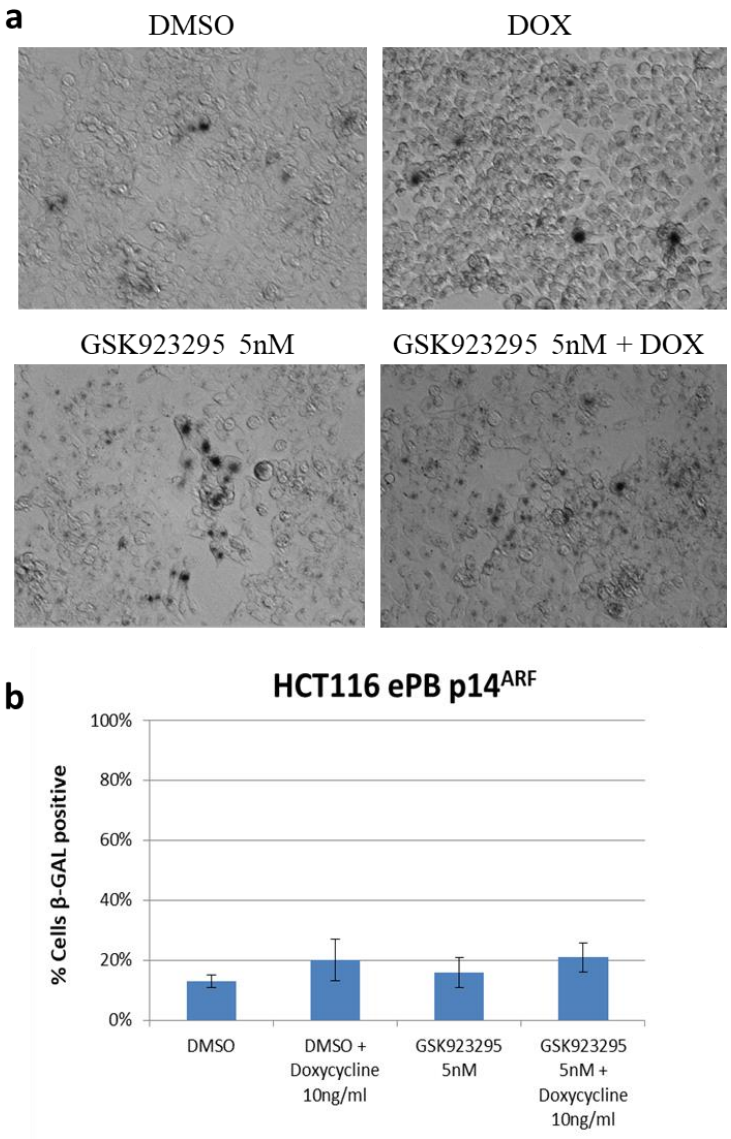

Fig. 33: p14^{ARF} does not induce cellular senescence in GSK923295 treated cells. On the top representative pictures of DMSO (Control), Doxycicline 10ng/ml, GSK923295 5nM and GSK+Dox HCT116 epB-p14 cells, 72 h after GSK treatment stained for β-gal. The graph on the bottom summarizes the percentage of senescent HCT116 cells (β-gal positive).The differences are not statistical significant.

To assess if apoptosis was responsible for observed reduction of aneuploid cells, I conducted the Acridine Orange/Ethidium Bromide (AO/EB) assay that distinguishes live cells from apoptotic and necrotic cells (Fig.34). I found a high percentage (25%) of apoptotic cells following $p14^{ARF}$ ectopic expression and GSK923295 treatment. The increase of the percentage of apoptotic cells and the reduction of aneuploid cells after $p14^{ARF}$ ectopic expression suggests apoptosis as a main mechanism to eliminate aneuploid cells.

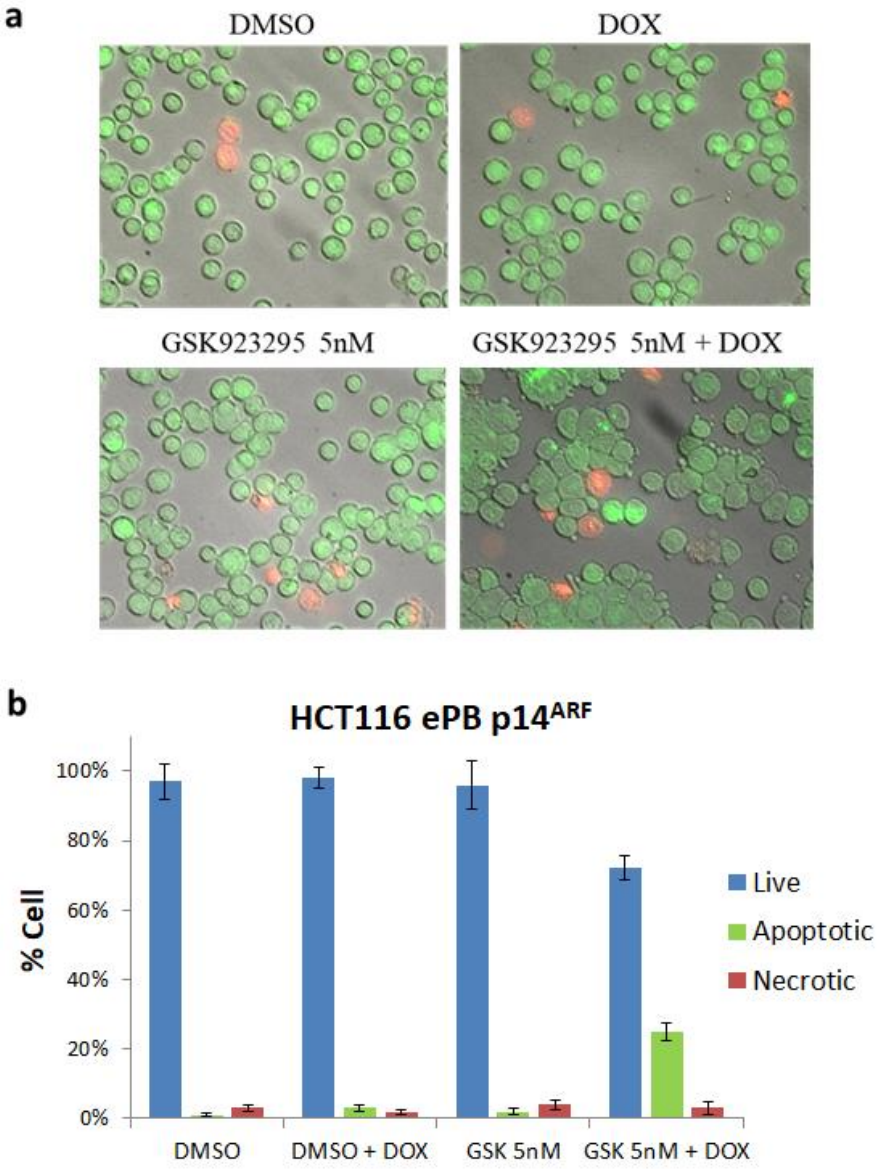

Fig.34 $p14^{ARF}$ ectopic expression induces apoptosis in GSK923295 treated HCT116 ePB-p14 cells. a: Examples of HCT116 cells stained with Orange Acridine and Ethidium Bromide 72 h after treatment; b: The graph summarizes the percentage of live, apoptotic and necrotic HCT116 ePB-$p14^{ARF}$ cells.

3 Transcriptomic analysis of aneuploid IMR90 cells induced by CENP-E depletion

CENP-E is an essential gene, CENP-E homozygous knockout (CENP-E-/-) mice undergo massive chromosome segregation defects and die at embryonic stage (Weaver et al.2007). On the contrary, heterozygous (CENP-E+/-) mice are viable even though they exhibit elevated levels of aneuploidy and develop spleen and lung cancer (Silk et al. 2013).

It has been shown that partial depletion of CENP-E in human primary fibroblasts (IMR90) triggered aneuploidy that is maintained for two weeks, suggesting that these cells have acquired traits that allow them to tolerate the adverse effects of chromosomal imbalances and to proliferate. However, we still lack complete knowledge of specific gene/s network/s that are responsible for inducing aneuploidy tolerance.

3.1 Transcriptome analysis of aneuploid induced fibroblasts

Here CENP-E was partially depleted by RNA interference in human primary fibroblasts (IMR90) and high-throughput gene expression profiling by DNA microarrays was done at "early" (72 hours post-RNAi) and "late" (2 weeks post-RNAi) time points to investigate what gene/networks are necessary for aneuploid human cells to cope with deleterious consequences of aneuploidy, considering that aneuploidy tolerance can be involved in tumorigenesis.

The technology chosen was the Agilent technologies and I performed the microarrays experiment using the Human Gene Expression 4x44K Microarray kit, a chip that target 19.596 Entrez Gene RNAs. Each RNA sample was first tested using the agilent Bioanalyzer instrument (Agilent) to assess its integrity.

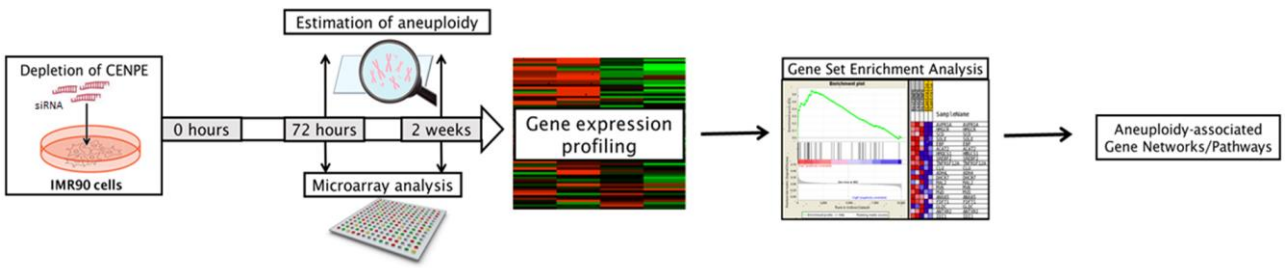

Fig. 35: Experimental scheme design.

Each RNA sample was labelled with Cytidine triphosphate (CTP) nucleotides conjugated with Cy3 and Cy5 according to the Agilent protocol. Because I analysed a number of samples of equal interest and high quality, I chose a design that utilizes a large number of direct sample-to-sample comparison.

I performed three microarray experiments, to have more significant data I made each microarray experiment with mRNA from a different sample (experiment replicate) (up to four experiment replicate for sample), and each sample was present in an array chip two times, one labelled with Cy3 and one labelled with Cy5 (internal instrument replicate). The Agilent Technologies G2505B Micro Array Scanner was used after the hybridization and then the Agilent Feature Extraction software generated raw data and Quality Control Report (Q.C.Report). The QC Report give some first information about the quality of the experiment, giving information of same particular spot of control that must be on or off, distribution of the fluorescent signal throughout the surface and other information about the experiment. The raw data were analysed using the GeneSpring software.

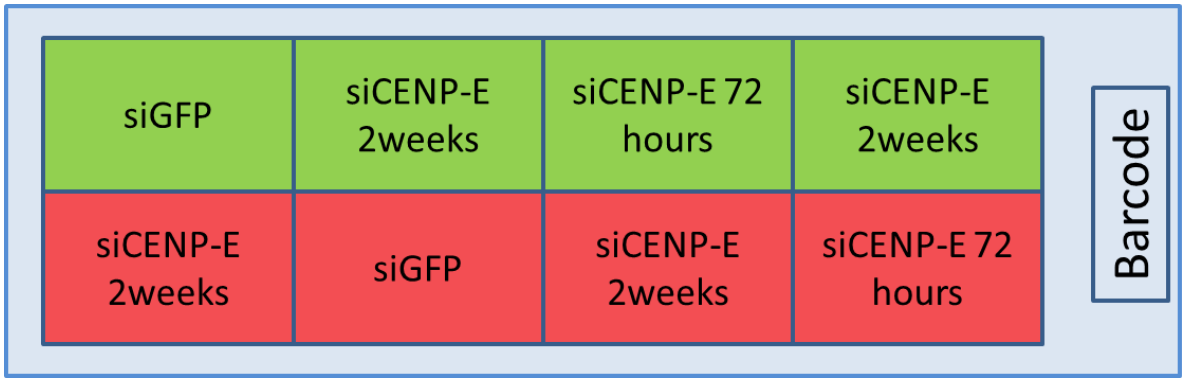

Figura 36: Organization of the samples in the RNA microarray chip. The green colour represents the samples labelled with Cy3, the red colour represent the samples labelled with Cy5.

3.2 De-regulated genes identification

These microarray analyses resulted in a list of genes found up or down regulated. I chose to focuses my attention to gene lists with a p-value less than 5% and with fold changes > 2 (log FC > 1). By this analysis the IMR90 siCENP-E 72 hours sample generated a higher

number of deregulated genes respect to the IMR90 siCENP-E 2 weeks sample. Fig. shows the graphs of significant deregulated genes found in the two samples.

By microarray analysis we identified 551 differentially expressed (DE) genes in IMR90 siCENP-E 72h and 222 DE genes in IMR90 siCENP-E 2 weeks compared to siGFP transfected cells (control). Raw data were exported to GeneSpring GX13.1. Hierarchical clustering was used to compare gene expression in each condition using default settings. The heatmap image was generated on the experiment conditions and classified on the basis of gene expression.

I identified deregulated genes that are common to IMR90 cells siCENP-E 72h and siCENP-E 2 weeks (Fig.). I found 56 annotated DEGs (Table 1) that shared by the two samples 29 upregulated and 19 downregulated in IMR90 siCENP-E 72h and 10 upregulated and 38 downregulated in IMR90 siCENP-E 2 weeks (Fig. 37).

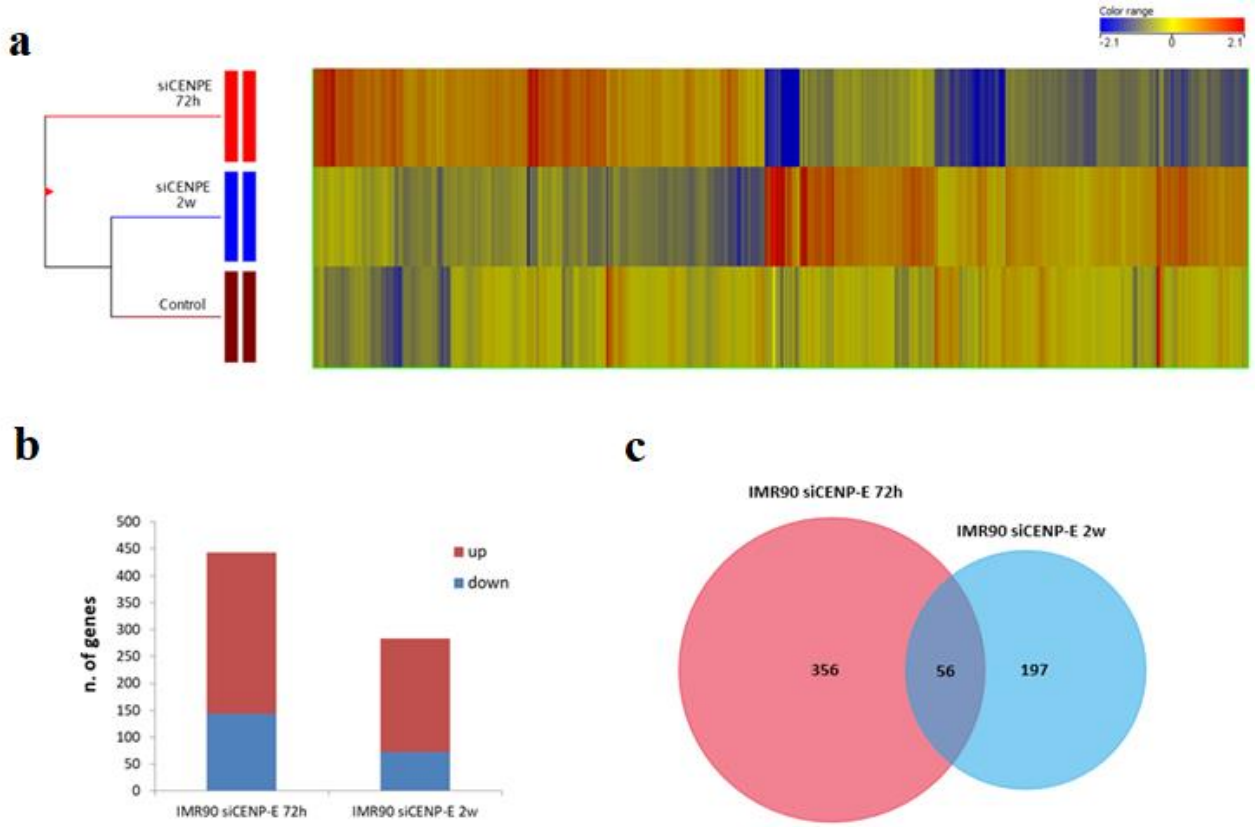

Fig. 3726: Comprehensive gene expression analysis in siCENP-E 72h and siCENP-E 2 weeks transfected IMR90 cells. (a) Unsupervised hierarchical clustering dendrogram, based on 609 differentially expressed and filtered probe-sets (FC ±2, p-value cut off ≤0.05), comparing IMR90 cells transfected with siGFP (control) and siRNA

targeting CENP-E 72 hours and 2 weeks after transfection. (b) Histogram showing number of genes up or down regulated in each sample. (c) Venn diagram showing the number common up- and down-regulated genes found in the indicated partially depleted IMR90 cells.

Table 1 : List of common deregulated genes (log FC >1) shared by IMR90 siCENP-E 72 hours and IMR90 siCENP-E 2 week samples

Gene symbol	Description	FC siCENP-E 72h	FC siCENP-E 2w	Chromosome	Map location
ANK3	ankyrin 3, node of Ranvier (ankyrin G)	-1,18	-1,42	10	10q21
AREG	amphiregulin	-1,12	2,45	4	4q13.3
BEX2	brain expressed X-linked 2	-1,39	-1,41	X	Xq22
BMP6	bone morphogenetic protein 6	-1,11	1,42	6	6p24-p23
CHRDL2	chordin-like 2	-2,08	1,51	11	11q14
CSGALNACT1	chondroitin sulfate N-acetylgalactosaminyltransferase 1	-1,42	1,93	8	8p21.3
EREG	epiregulin	-1,23	1,18	4	4q13.3
FOS	FBJ murine osteosarcoma viral oncogene homolog	-2,20	-4,20	14	14q24.3
FOSB	FBJ murine osteosarcoma viral oncogene homolog B	-1,86	-3,06	19	19q13.32
HBG1	hemoglobin, gamma A	-2,64	2,24	11	11p15.5
IRX2	iroquois homeobox 2	-2,30	-1,04	5	5p15.33
PDE4D	phosphodiesterase 4D, cAMP-specific	-1,94	1,45	5	5q12
RGS18	regulator of G-protein signaling 18	-2,24	1,90	1	1q31.2
SLC35F3	solute carrier family 35, member F3	-1,88	2,01	1	1q42.2
SLC4A4	solute carrier family 4 (sodium bicarbonate cotransporter), member 4	-1,10	1,01	4	4q21
SMOC1	SPARC related modular calcium binding 1	-1,59	2,35	14	14q24.2
SYNPO2	synaptopodin 2	-1,15	1,48	4	4q26
TFPI2	tissue factor pathway inhibitor 2	-1,55	2,40	7	7q22
TMEM155	transmembrane protein 155	-1,33	1,03	4	4q27
AOC3	amine oxidase, copper containing 3	1,55	1,60	17	17q21
ASAH1	N-acylsphingosine amidohydrolase (acid ceramidase) 1	1,31	1,88	8	8p22
BCL2L11	BCL2-like 11 (apoptosis facilitator)	1,53	1,36	2	2q13
C18orf54	chromosome 18 open reading frame 54	1,04	1,07	18	18q21.2
C1orf116	chromosome 1 open reading frame 116	1,45	1,60	1	1q32.1
CLEC2D	C-type lectin domain family 2, member D	1,63	1,27	12	12p13
CNIH3	cornichon family AMPA receptor auxiliary protein 3	1,89	-1,29	1	1q42.12
COQ9	coenzyme Q9	1,17	1,40	16	16q21
CRH	corticotropin releasing hormone	1,12	-1,07	8	8q13
DENND2C	DENN/MADD domain containing 2C	1,49	1,05	1	1p13.2
IL1RAP	interleukin 1 receptor accessory protein	1,09	1,23	3	3q28
KCNMA1	potassium channel, calcium activated large conductance subfamily M alpha, member 1	1,91	-1,20	10	10q22.3
MX1	MX dynamin-like GTPase 1	1,10	-1,25	21	21q22.3
NIPAL2	NIPA-like domain containing 2	1,41	1,49	8	8q22.2
PDE1A	phosphodiesterase 1A, calmodulin-dependent	1,17	1,81	2	2q32.1
PEAK1	pseudopodium-enriched atypical kinase 1	1,08	1,03	15	15q24.3
PGK1	phosphoglycerate kinase 1	1,49	1,58	X	Xq13.3
PRUNE2	prune homolog 2 (Drosophila)	1,74	1,19	9	9q21.2
PTGFR	prostaglandin F receptor (FP)	1,09	1,33	1	1p31.1
RGS4	regulator of G-protein signaling 4	1,32	-1,30	1	1q23.3
RHOT1	ras homolog family member T1	1,58	1,10	17	17q11.2
SCN7A	sodium channel, voltage gated, type VII alpha subunit	1,15	1,14	2	2q21-q23
SEMA3D	sema domain, immunoglobulin domain (Ig), short basic domain, secreted, (semaphorin) 3D	1,31	1,25	7	7q21.11
SPOCK2	sparc/osteonectin, cwcv and kazal-like domains proteoglycan (testican) 2	1,17	1,41	10	10pter-q25.3
TANC2	tetratricopeptide repeat, ankyrin repeat and coiled-coil containing 2	1,48	1,35	17	17q23.3
TAS2R19	taste receptor, type 2, member 19	1,52	2,00	12	12p13.2
TTC23	tetratricopeptide repeat domain 23	1,39	1,25	15	15q26.3
USP2	ubiquitin specific peptidase 2	1,12	1,09	11	11q23.3
ZC3H13	zinc finger CCCH-type containing 13	1,14	2,12	13	13q14.13

3.2 Validation of arrays data using RT-qPCR analysis

I validated the observed gene expression changes by RT-qPCR in independent biological replicates of IMR90 cells treated with the CENP-E siRNA under the same conditions used for the microarrays. Seven deregulated genes were selected for RT-qPCR analysis: TFPI2, DUSP6, BTG2, CYFIP2, KLF4, CEP131 and CHAMP1 (Fig.). Gene fold changes resulting

from RT-qPCR were mostly in agreement with the microarray data.

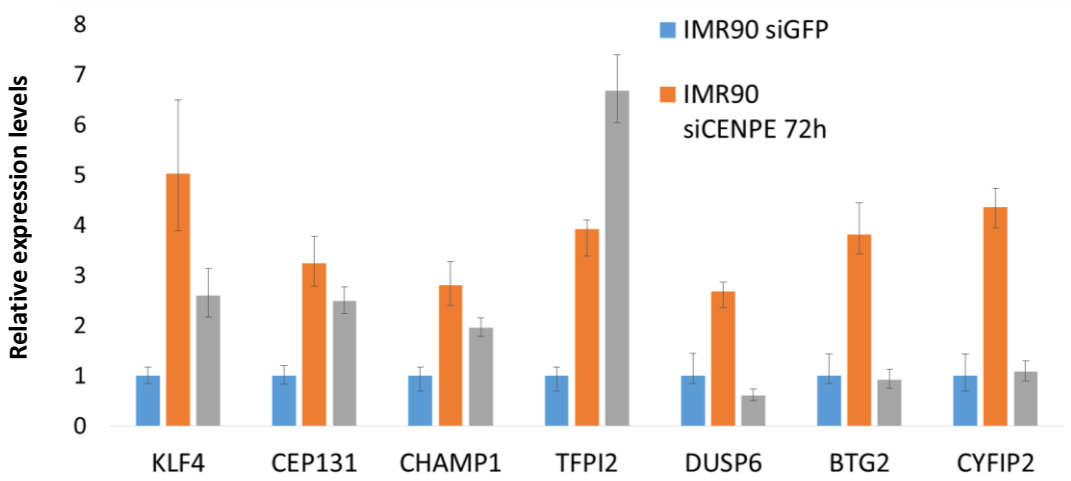

Fig. 3827: RT-qPCR results from siCENP-E 72h and siCENP-E 2weeks IMR90 cells, compared to IMR90-siGFP transfected cells. The assays were performed in quadruplicates and repeated in three independent experiments. The data are presented as the mean ± SD (error bar) of fold-change.

3.3 Gene Set Enrichment Analysis (GSEA) analysis

Normalized data were also analysed with the GSEA web-tool (www.broadinstitute.org/gsea) to detect the pathways/gene-sets significantly deregulated in each treatment (with respect to the control (siGFP). These analysis revealed pathways altered in the two samples. The Tables 2-3 show the significant (FDR q-value < 0.2) deregulated GSEA Gene-Sets (Hallmark). The only altered pathway shared between the two sample resulted Xenobiotic metabolism gene set which resulted downregulated in early aneuploid cells (IMR90 siCENP-E 72 hours) and up-regulated in late aneuploid cells (IMR90 siCENP-E 2 weeks).

Since most of the altered pathways were found not to be shared between the two samples, I further investigated gene lists inside this deregulated pathways to check deregulated common genes, despite being included in different gene sets. I found 52 genes shared between the two samples (Table 4), 5 resulted up-regulated and 14 down-regulated in both samples, while the remaining 32 genes were differently altered at 72 hours and at 2 weeks.

The only pathways significantly up-regulated in IMR90 siCENP-E 72h were *Apoptosis* and *Cholesterol Homeostasis* gene-sets, conversely most of the altered pathways resulted down-regulated.

IMR90-siCENPE 2w cells, showed up-regulation in Epithelial-mesenchymal transition, Hypoxia and Xenobiotic metabolism gene-sets and at the same time the down-regulation of P53 pathway, that usually are correlated with tumor progression and metastasis.

Table 2 : Gene sets enriched in phenotype **siCENPE 72h** (FDR q-value<0,2)

CENPE 72h	
Gene-set Name	**Enrichment Score**
HALLMARK_CHOLESTEROL_HOMEOSTASIS	0.550825
HALLMARK_APOPTOSIS	0.29306307
HALLMARK_E2F_TARGETS	-0.4112242
HALLMARK_G2M_CHECKPOINT	-0.42952272
HALLMARK_MITOTIC_SPINDLE	-0.33654705
HALLMARK_ANGIOGENESIS	-0.44820115
HALLMARK_ESTROGEN_RESPONSE_LATE	-0.30400178
HALLMARK_BILE_ACID_METABOLISM	-0.33262056
HALLMARK_XENOBIOTIC_METABOLISM	-0.29437807
HALLMARK_UNFOLDED_PROTEIN_RESPONSE	-0.31752646
HALLMARK_ADIPOGENESIS	-0.29467914
HALLMARK_TNFA_SIGNALING_VIA_NFKB	-0.28777105

Table 3 : Gene sets enriched in phenotype **siCENPE 2w** (FDR q-value<0,2)

CENPE 2w	
Gene-set Name	**Enrichment Score**
HALLMARK_EPITHELIAL_MESENCHYMAL_TRANSITION	0.33510843
HALLMARK_IL6_JAK_STAT3_SIGNALING	0.37629685
HALLMARK_INTERFERON_GAMMA_RESPONSE	0.33727473
HALLMARK_HYPOXIA	0.34279573
HALLMARK_XENOBIOTIC_METABOLISM	0.31554386
HALLMARK_COAGULATION	0.32489774
HALLMARK_HEME_METABOLISM	0.30528104
HALLMARK_COMPLEMENT	0.31029537
HALLMARK_HEDGEHOG_SIGNALING	0.41114244
HALLMARK_INFLAMMATORY_RESPONSE	0.30268276
HALLMARK_UV_RESPONSE_DN	0.3095823
HALLMARK_ALLOGRAFT_REJECTION	0.2876117
HALLMARK_MTORC1_SIGNALING	-0.33381698
HALLMARK_P53_PATHWAY	-0.34690675
HALLMARK_NOTCH_SIGNALING	-0.45094362
HALLMARK_KRAS_SIGNALING_UP	-0.29774994

Upregulated gene-sets Downregulated gene-sets

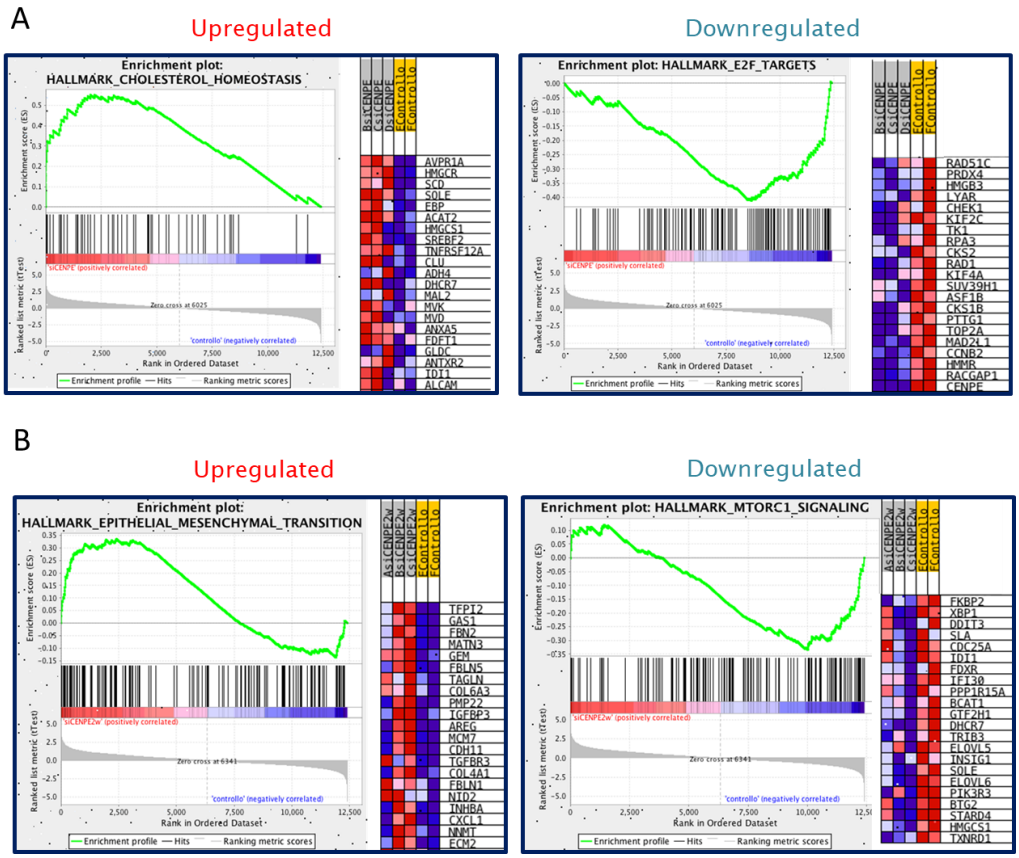

Fig. 39: The Gene Set Enrichment Analysis (GSEA) tool was used to identify gene-sets that were differentially expressed in IMR90 cells at 72h and two weeks after CENP-E post-transcriptional silencing. A-B) ES curve (green) of the running sum of the weighted enrichment score obtained with GSEA for 2 gene-sets significantly overexpressed and underexpressed in the two samples

Table 4 : List of common deregulated genes present in the alterated gene sets shared by IMR90 siCENP-E 72 hours and IMR90 siCENP-E 2 week samples

Deregulated genes shared by the two samples	72h		2w		
ANXA5	CHOLESTEROL HOMEOSTASIS		COMPLEMENT		
ADD1	APOPTOSIS		HEME METABOLISM		
CD38	APOPTOSIS		IL6 JAK STAT3 SIGNALING	INTERFERON GAMMA RESPONSE	
PDGFRB	APOPTOSIS		EPITHELIAL MESENCHYMAL TRANSITION		UV RESPONSE DN
PSEN1	APOPTOSIS		COMPLEMENT	INFLAMMATORY RESPONSE	
BNIP3L	APOPTOSIS		HEME METABOLISM	HYPOXIA	
TFRC	E2F TARGETS		HEME METABOLISM		
FSTL1	ANGIOGENESIS		EPITHELIAL MESENCHYMAL TRANSITION		
LUM	ANGIOGENESIS		EPITHELIAL MESENCHYMAL TRANSITION		
TNFRSF21	ANGIOGENESIS		IL6 JAK STAT3 SIGNALING		
COL5A2	ANGIOGENESIS		EPITHELIAL MESENCHYMAL TRANSITION		UV RESPONSE DN
AREG	ESTROGEN RESPONSE LATE	TNFA SIGNALING VIA NFKB	EPITHELIAL MESENCHYMAL TRANSITION		
CXCL12	ESTROGEN RESPONSE LATE		EPITHELIAL MESENCHYMAL TRANSITION		
TFPI2	ESTROGEN RESPONSE LATE		EPITHELIAL MESENCHYMAL	COAGULATION	COMPLEMENT
WISP2	ESTROGEN RESPONSE LATE		HYPOXIA		
GCLM	BILE ACID METABOLISM		HEME METABOLISM		
ISOC1	BILE ACID METABOLISM		INTERFERON GAMMA RESPONSE		
AKR1C2	XENOBIOTIC METABOLISM		XENOBIOTIC METABOLISM		
ATOH8	XENOBIOTIC METABOLISM		XENOBIOTIC METABOLISM		
MAOA	XENOBIOTIC METABOLISM		XENOBIOTIC METABOLISM		
TPST1	XENOBIOTIC METABOLISM		XENOBIOTIC METABOLISM		
TYR	XENOBIOTIC METABOLISM		XENOBIOTIC METABOLISM	HEME METABOLISM	
CCL2	UNFOLDED PROTEIN RESPONSE	TNFA SIGNALING VIA NFKB	INTERFERON GAMMA RESPONSE	INFLAMMATORY RESPONSE	
CEBPB	UNFOLDED PROTEIN RESPONSE	TNFA SIGNALING VIA NFKB	COMPLEMENT		
ALDH2	ADIPOGENESIS		XENOBIOTIC METABOLISM		
FOSL2	TNFA SIGNALING VIA NFKB		HYPOXIA		
IL1B	TNFA SIGNALING VIA NFKB		IL6 JAK STAT3 SIGNALING		
PDE4B	TNFA SIGNALING VIA NFKB		INTERFERON GAMMA RESPONSE		
PPAP2B	TNFA SIGNALING VIA NFKB		UV RESPONSE DN		
SOCS3	TNFA SIGNALING VIA NFKB		IL6 JAK STAT3 SIGNALING	INTERFERON GAMMA RESPONSE	
TNFAIP6	TNFA SIGNALING VIA NFKB		INTERFERON GAMMA RESPONSE	INFLAMMATORY RESPONSE	
DHCR7	CHOLESTEROL HOMEOSTASIS		MTORC1 SIGNALING		
HMGCS1	CHOLESTEROL HOMEOSTASIS		MTORC1 SIGNALING		
IDI1	CHOLESTEROL HOMEOSTASIS		MTORC1 SIGNALING		
SQLE	CHOLESTEROL HOMEOSTASIS		MTORC1 SIGNALING		
BIRC3	APOPTOSIS		KRAS SIGNALING UP		
BTG2	APOPTOSIS		MTORC1 SIGNALING	P53 PATHWAY	
DDIT3	APOPTOSIS		MTORC1 SIGNALING	P53 PATHWAY	
DCXR	ESTROGEN RESPONSE LATE	XENOBIOTIC METABOLISM	P53 PATHWAY		
ELOVL5	ESTROGEN RESPONSE LATE	XENOBIOTIC METABOLISM	MTORC1 SIGNALING		
HSPA4L	ESTROGEN RESPONSE LATE		P53 PATHWAY		
ST14	ESTROGEN RESPONSE LATE		P53 PATHWAY		
TOB1	ESTROGEN RESPONSE LATE	ADIPOGENESIS	P53 PATHWAY		
TSPAN13	ESTROGEN RESPONSE LATE		KRAS SIGNALING UP		
PPARD	XENOBIOTIC METABOLISM		NOTCH SIGNALING		
EDEM1	UNFOLDED PROTEIN RESPONSE		MTORC1 SIGNALING		
SERP1	UNFOLDED PROTEIN RESPONSE		MTORC1 SIGNALING		
SLC1A4	UNFOLDED PROTEIN RESPONSE		MTORC1 SIGNALING		
RETN	ADIPOGENESIS		KRAS SIGNALING UP		
HES1	TNFA SIGNALING VIA NFKB		NOTCH SIGNALING		
IER3	TNFA SIGNALING VIA NFKB		P53 PATHWAY		
IER5	TNFA SIGNALING VIA NFKB		P53 PATHWAY		

3.4 Tissue factor pathway inhibitor 2 (TFPI2) as putative aneuploidy inhibitor

Looking for candidate genes involved in aneuploidy promotion and tolerance mechanisms, I focused on Tissue Factor Pathway Inhibitor 2 (TFPI2), included among genes previously validated by RT-qPCR that resulted greatly up-regulated in IMR90 siCENP-E at 72h from transfection. TFPI-2 is a Kunitz-type proteinase inhibitor that acts against a wide range of serine proteases (Chand HS et al. 2004). TFPI-2 expression plays a significant role in inhibiting tumor invasion and metastasis (Konduri SD et al. 2001) and it has been shown that TFPI2 is more frequently methylated in well-differentiated advanced colorectal and gastric carcinomas (Hibi et al. 2010). Moreover, TFPI2 restoration in a highly invasive glioblastoma cell line induces both intrinsic and extrinsic caspase-mediated pathway leading to apoptosis (George J et al. 2007). These findings suggest that TFPI2 may act as a tumour suppressor and its methylation may present a potential risk of malignancy in different cancer.

To test if TFPI2 is involved in aneuploidy promotion IMR90 cells were transfected with a TFPI2 specific siRNAs (siTFPI2) and with an unspecific siRNA targeting the green fluorescent protein (siGFP) as a control. RT-qPCR analysis (Fig.) to quantify the levels of TFPI2 transcript at 72 hours after RNAi, showed reduction of the TFPI2 mRNA in IMR90 cells. RNAi of TFPI2 lowered the TFPI2 transcript at the basal level also in IMR90 siCENP-E transfected cells (Fig.40).

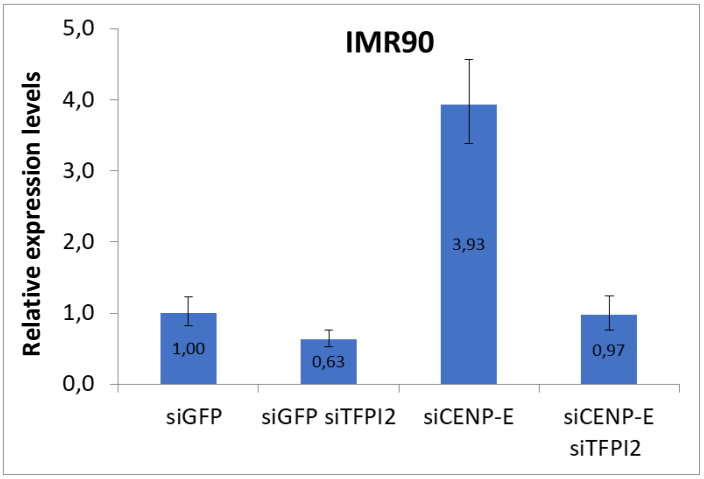

Fig. 40: RT-qPCR showing TFPI2 transcript levels in IMR90 at 72 h after transfection with the following siRNAs: siGFP, siGFP/siTFPI2, siCENP-E, siCENP-E/siTFPI2.

I analysed then these siRNA transfected cells by cytogenetic assay to verify effects on the cellular ploidy. At 72 hour post-transfection, RNA interfered TFPI2 cells showed an increased fraction of aneuploid cells (57%) compared to IMR90 control cells (19%). More interestingly, double-depleted CENP-E/TFPI2 cells showed an increased fraction of aneuploid cells (76%) compared to the percentage of aneuploid cells CENP-E depleted (56%) (fig.41) thus suggesting a role for TFPI2 in counteracting aneuploid cell proliferation. In addition also TFPI2 inhibition alone induced aneuploidy, These results suggest that the tumor suppressor function of TFPI-2 could be related to the control of aneuploid cells proliferation.

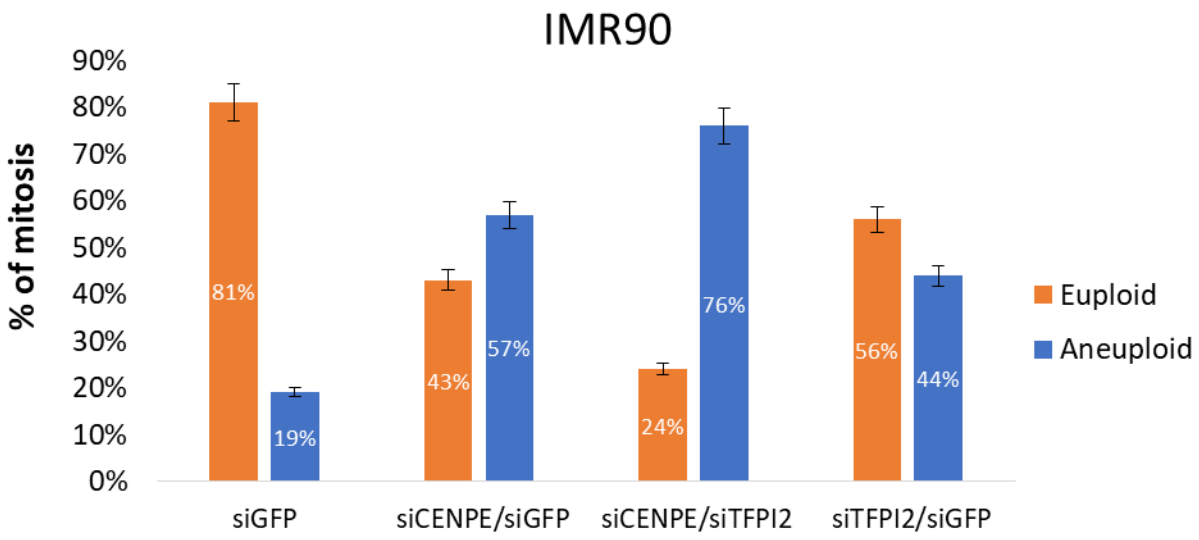

Fig. 41: Metaphase spreads analysis showing the effects of simultaneous depletion of CENP-E and TFPI2 in IMR90 cells.

CONCLUSIONS

Aneuploidy is not well tolerated in higher eukaryotes and represents one of the main causes of spontaneous abortions in humans and the surviving children suffer from severe developmental disabilities (Colnaghi et al, 2011). Furthermore, aneuploidy is found in 90% of solid tumors and increased rates of aneuploidy in cancers correlate with poor prognosis and drug resistance (Birkbak et al. 2011; Lee et al. 2011). Although the phenotypes caused by altered chromosome numbers are widely described, the underlying mechanisms of the physiological consequences of aneuploidy remain poorly understood.

In this thesis, I studied the mechanisms that could determine the promotion and tolerance of aneuploidy in human cells. In particular I induced aneuploidy, in IMR90 primary human fibroblasts and in near diploid cell line (HCT116) lacking $p14^{ARF}$ tumor suppressor, by weakening the CENP-E motor protein required for stable spindle microtubule capture at kinetochores.

CENP-E partial depletion has not relevant influence on cell proliferation of both kind of cells but induced mitotic abnormalities like monopolar spindle and lagging chromosomes that could explain the aneuploidy generation as seen in mouse embryonic fibroblasts (Silk et al. 2013). It was reported that aneuploid cells are outcompeted by normal cells in culture (Thompson & Compton 2010) and do not exist data about the fate of induced aneuploid cells at longer times than 72 hours from induction. Also in this case, the two different cell types responded differently. At four weeks after CENP-E depletion aneuploidy returned at normal levels in human primary fibroblasts IMR90 cells while HCT116 cells showed still aneuploid cells although the percentage of aneuploidy decreased when compared to that at 72 hours. The finding that aneuploid cells were found up to two weeks in IMR90 cells suggests that a threshold level of $p14^{ARF}$ protein must be reached to activate a pathway that block aneuploid cells proliferation (Groth et al. 2000). Also, it is interesting to notice that IMR90 cells were still aneuploid at two weeks after CENP-E depletion but with a different profile showing a marked decrease of hyperdiploid cells. Probably, the tumor suppressor $p14^{ARF}$ is able to counteract hyperdiploidy in agreement with other data showing that loss of ARF is sufficient to increase the number of near tetraploid cells in the mouse (Britigan et al. 2014). The increased $p14^{ARF}$ expression levels at 72 hours, 2 weeks and 4 weeks after CENP-E silencing and the simultaneous aneuploidy decrease in IMR90 cells suggested the involvement of the tumor suppressor to limit aneuploid cells proliferation.

Interestingly, aneuploidy induced by CENP-E partial depletion or inhibition was not tolerated in HCT116 cells re-expressing $p14^{ARF}$. This finding strongly suggests that $p14^{ARF}$ blocked aneuploid cell proliferation. The induction of $p14^{ARF}$ trough Doxycycline with two different expression systems (pBPSTR1 Tet-OFF retroviral vector and Piggybac Tet-ON transposon vector) decreased aneuploid cell numbers suggesting that aneuploidy development is influenced by p14ARF expression levels. Generally, gene expression correlates with gene copy number. The imbalance of gene expression induced by aneuploidy could then induce a signal resembling hyperproliferative stress typically sensed by $p14^{ARF}$ that could activate p53-dependent apoptosis, as previously described (Williams et al. 2008). Taken together, these results reinforce the idea that loss of $p14^{ARF}$ expression or $p14^{ARF}$ related partners that control genomic stability is one of the strategies adopted by human tumor cells to cope with aneuploidy.

Another important aspect in the aneuploid field is the identification of deregulated pathways/genes that could shed light on genes involved in inducing as well in maintaining aneuploidy. Identifying these differences is crucial for understanding the impact of aneuploidy on tumorigenesis.

To this aim I studied the gene expression profiles of aneuploid human primary fibroblasts following CENP-E partial depletion to elucidate the possible existence of a molecular signature triggering aneuploidy and its tolerance. I analyzed gene expression profiles of early (IMR90 siCENP-E 72 hours) and late (IMR90 siCENP-E 2 weeks) aneuploid cells. I did a detailed analysis of transcriptional changes occurring in aneuploid human primary fibroblasts by DNA microarray. By using bioinformatic tools (GeneSpring and GSEA) it was possible to list several differentially expressed genes and then generate a sub-list of common expressed genes, pathways and regulatory factors. Some of these differentially expressed genes were validated by RT-qPCR.

“Early” (72 h) gene set analysis showed *Apoptosis* and *Cholesterol Homeostasis* gene-sets up-regulated, these pathways could be activated by the cells as a stress response to aneuploidy induction.

Hypoxia in the tumor microenvironment enhances tumor progression (Huang et al. 2007) and it has been shown that hypoxia induces chromosomal abnormalities in endothelial cells through the induction of reactive oxygen species (ROS) and excess signalling of vascular endothelial growth factor (VEGF) in the tumor microenvironment (Kondoh et al. 2013).

Interestingly, “Late” (2 weeks) gene set analysis showed enrichment in Epithelial-mesenchymal transition, Hypoxia and Xenobiotic metabolism gene-sets that are correlated with tumor progression and metastasis.

Our work for the first time identifies genes/pathways altered in human primary fibroblasts becoming aneuploid by posttranscriptional silencing of a single gene involved in chromosome segregation (CENP-E). It could be interesting to evaluate the role of these pathways/genes in the aneuploidy tolerance and evaluate if these pathway where deregulated also in other cell lines chromosomally instable to identify molecular target for treatment of cancer cells.

MATERIALS AND METHODS

Cells and cell culture

Human primary fibroblasts (IMR90, ATCC) were cultured in EMEM supplemented with: 10% FBS (GIBCO, Invitrogen, Monza Italy), 100units/ml penicillin and 0, 1 mg/ml streptomycin, 1% NEAA; Colon cancer cells HCT116 with MIN phenotype (near-diploid cells) HCT116 cells (kindly provided by Dr. B. Vogelstein, John Hopkins University, Baltimore, MD) were cultured in D-MEM with 10% FBS (GIBCO, Invitrogen, Monza, Italy), 100 U/ml penicillin and 0.1 mg/ml streptomycin. Cells were cultured in a humidified atmosphere of 4% CO_2 in air at 37° C. GSK923295 (Selleckchem) dissolved in DMSO was used at the final concentration of 5nM for 72 hours. To modulate the $p14^{ARF}$ expression I used doxycycline at the final concentration of 10ng/mL to obtain the expression of $p14^{ARF}$ (TET ON system).

Cell transfection and RNA interference

Transient transfection was performed on cells seeded the previous day to reach 70% confluence on the day of transfection. HCT116 cells were transfected with the siRNA (5′GGC UAC GUC CAG GAG CGC ACC-3′) targeting GFP (control) and siRNA#1 (5′-AAG CAG AGA GAA GGG UGA ACC-3′) targeting CENP-E both at the final concentration of 60 nM. Stable transfection, HJCT116 cells were co-transfected with the ePB-sd-TT plasmid empty or harboring the $p14^{ARF}$ c-DNA and the hyPB transposase vector (kindly provided by Dr. Ali Brivanlou, The Rockefeller University, New York, USA). After 48 hours from transfection cells were selected with blasticidine (400µg/ml). IMR90 cells were transfected with control siRNA (GFP) and CENP-E siRNA#2 (5′–AAC GAA GAG UUA CUU GGU GCC–3′) at the final concentration of 40 nM. For the double knockdown experiment, CENP-E siRNA#2 and the siRNA targeting $p14^{ARF}$ (5′- GAA GAU CAG GUC AUG AUG ATT-3′) were co-transfected at a final concentration of 40 nM. For TFPI2 knockdown, IMR90 were transfected with a specific siRNA (5′- GCA UGA GGA AAC AAA UCA U - 3′) at the final concentration of 40 nM Transfection was done using Lipofectamine 2000 (Thermo Fisher Scientific, Monza, Italy) according to the manufacturer's protocol. Briefly, on the day of transfection the siRNA, the plasmid DNA and the transfection reagent (Lipofectamine 2000,

Thermo Fisher Scientific, Monza, Italy) were diluted separately in Opti-MEM (GIBCO, Thermo Fisher Scientific, Monza, Italy), mixed gently and then incubated for 5 min at room temperature. After incubation, the siRNA and the plasmid DNA were mixed with Lipofectamine 2000 (Thermo Fisher Scientific, Monza, Italy), for 30 min at room temperature to allow complex formation, and added to the plates containing 2 ml of culture medium. After 6 h at 37 °C, the transfection medium was replaced with fresh medium and cells were further cultured for 72 h. To switch off $p14^{ARF}$ transgene expression in the HCT116 transfected cells (Tet-ON system) doxycycline was added at a final concentration of 10ng/ml 24 hours.

Construction of the expression vector

To obtain inducible expression of $p14^{ARF}$ in HCT116 cells, we used the ePB transposon vector (Tet-ON). The fragment containing the $p14^{ARF}$ cDNA was cut from the pBPSTR1 retroviral vector using BamHI and NotI restriction enzymes. The BamHI-NotI fragment was then inserted into the ePB vector previously digested with BamHI and NotI. DNA sequencing of the construct was used to confirm the presence of the insert and its correct orientation.

Purification of $p14^{ARF}$ c-DNA from pBPSTR1

An aliquot of pBPSTR1-p14 vector was subjected to double digestion using the restriction enzymes BamHI and NotI to isolate the c-DNA. The reaction mixture (Vf =100µL) contained:

- 20µg pBPSTR1
- 5µl BamHI (10u/µl)
- 5µl NotI (10u/µl)
- 10µl Buffer Tango 10x
- 60µl H2O DNAsi/RNAsi free
-

The mixture was incubated at 37°C for 2 hours.

Electrophoresis on 1% agarose gel, with ethidium bromide (0,5µg / ml) in TAE buffer (40mM Tris-acetate, 1mM EDTA), was used to purify the correspondent band of $p14^{ARF}$ c-DNA (≈

500bp) with PureLink Quick Gel Extraction Kit extraction PCR Purification COMBO kit (Invitrogen).

Digestion, de-phosphorylation and purification of ePB vector

An aliquot of ePB vector was subjected to digestion using the restriction enzymes PmeI to obtain blunt end for 2 hours at 37°C. The reaction mixture was performed with:

- 3,5µg DNA
- 1µl BamHI (10u/µl)
- 1µl NotI (10u/µl)
- 2µl Buffer Tango 10x
- 12,5µl H2O

Then the vector was precipitate with NaAc 0,3M ed EtOH, suspended in 20 µl of TE buffer and dephosphorylated with alkaline phosphatases of calf intestine (CIAP). The mixture was incubated at 50°C for 10 minutes and then at 68°C for 10 minutes. The vector was purified with phenol-chloroform protocol and precipitated with NaAC 0.3M and absolute EtOH.

Quantification of $p14^{ARF}$ c-DNA and ePB vector

ePB vector and $p14^{ARF}$ c-DNA was subjected to electrophoresis on 1% agarose gel, with ethidium bromide (0,5µg / ml) in TAE buffer (40mM Tris-acetate, 1mM EDTA), and quantized using 2-Log DNA Ladder 100ng/µl (New England Biolabs).

Ligation reaction between $p14^{ARF}$ c-DNA and ePB vector

The ligation mix was performed in 20µl using a molar ratio of 1:5 vector to insert:

- 0,5µl ePB vector BamHI / XbaI double digested
- 6µl of c-DNA BamHI / XbaI double digested

- 2µl di Buffer
- 0,5µl di Ligase
- 11µl H2O
-

Reaction incubated at 12°C o.n.

Transformation of E. Coli with ePB-p14^{ARF} construct

The ligase mixture was used for transformation of competent cells of E. coli (TOP10 strain) using thermal shock protocol. The suspension was seeded in a Petri dish containing agar supplemented with ampicillin 100µg/ml and incubated overnight at 37°C in order to select the transformed bacteria. From the transformation several colonies were obtained, subsequently subjected to a colony PCR reaction with primers specific for the vector sequences and the insert.

For the colony PCR, part of the colony was picked from the plate and dissolved in sterile H2O in a PCR tube. After the first step at 95 ° C for 3 minutes, to take place lysis of bacterial cells, it was added 20µl of reaction mixture:

- 12,5µl REDTaq ReadyMix PCR Reaction Mix con MgCl2 (Sigma Aldrich Inc.)
- 1,25µl primer Fw 4µM
- 1,25µl primer Rv 4µM
- 5µl H2O

Thermic profile:

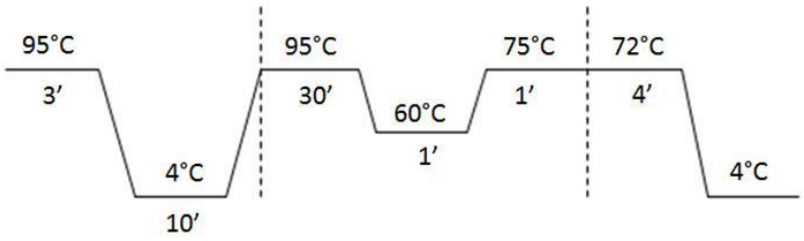

Oligo	Sequence 5’-3’
P14-Fw	GGTTTTCGTGGTTCACATCCCGC
P14-Rev	CAGGAAGCCCTCCCGGGCAGC

Cell viability

To assess cell viability cells were transfected with the specific siRNA plasmids for 24h, 48h and 72h, harvested by trypsinization and collected in a tube with 4ml of phosphate buffered saline (PBS). Cell suspensions (100 ml) were mixed with 100 ml of Trypan Blue (Sigma–Aldrich, Milan, Italy) and 10ml were placed in a Burker chamber for cell counting.

Real time qRT-PCR

Primers to be used in Real-Time qRT-PCR experiments were designed with Primer Express software (Applied Biosystems, Monza, Italy) choosing amplicons of 70–100 bp. The selected sequences were tested against public databases (BLAST) to confirm the identity of the genes. Total RNA was extracted from cells by using the RNAeasy Mini kit according to the manufacturer’s instruction (Qiagen, Milan, Italy). RNA was reverse-transcribed in a final volume of 40ml using the High Capacity c-DNA Archive kit (Applied Biosystems) for 10 min at 25°C and 2 h at 37°C. Real-Time qRT-PCR reaction was performed as previously described (Barra et al. 2012). Real-Time qRT-PCR was done in a final volume of 20 µl comprising 1X Master Mix SYBR Green (Applied Biosystems) and 0.3mM of forward and reverse primers.

Gene	Forward primer	Reverse primer
GAPDH	5’-CTCATGACCACAGTCCATGCC-3’	5’-CAATCCACAGTCTTCTGGGT-3’
CENP-E	5’-GTGGGACCAGTTCAGCCTGATA-3’	5’-GATGTGAACCACGAAAACCCTC-3’
DUSP6	5’-AACAGGGTTCCAGCACAGCAG-3’	5’-GGCCAGACACATTCCAGCAA-3’
BTG2	5’-CTCCATCTGCGTCTTGTACGA-3’	5’-AGACTGCCATCACGTAGTTCT-3’
CYFIP2	5’-TCCGTATCCACCGTCCAAT-3’	5’-AATCTCCAGCAGCCACTCC-3’
KLF4	5’-GCAATATAAGCATAAAAGATCACC-3’	5’-AACCAAGACTCACCAAGCACC-3’
CEP131	5’-3’-CCATCACAGGGGCAGATACG-3’	5’-CTTTGTAGCTTGGCCTCCGA-3’

CHAMP1	5’-ATCCCAAACCCCAGAAGCAG-3’	5’-GGATGGTCCCCAAGGTTCTG-3’
TFPI2	5’-AACGCCAACAATTTCTACACCT-3’	5’-TACTTTTCTGTGGACCCCTCAC-3’

Western Blotting

Protein concentration was measured using the Bio-RadProtein Assay (Bio-Rad, Milan, Italy). Proteins (50mg) were separated by 3-8% and 10% SDS-PAGE containing 0.1% SDS and transferred to Hybond-C nitrocellulose membranes (Amersham Life Science, LittleChalfont, England) by electroblotting. The membranes were sequentially incubated with primary antibodies against CENP-E (C5) (Santa Cruz Biotechnology, Heidelberg, Germany), $p14^{ARF}$ (rabbit, anti-CDKN2A/P14ARF ab185620) and HRP-conjugated mouse (ab6789, Abcam, Cambridge, UK), or rabbit (ab97110, Abcam, Cambridge, UK) as secondary antibodies. The target protein was detected with enhanced chemiluminescence Western blotting detection reagents (Pierce, Milan, Italy). Membranes were stained by Ponceau-Red to confirm equivalent loading of total protein in all lanes. We used antibody against b-tubulin (mouse, SIGMA, Milan, Italy, 1:10,000) to confirm proteins loading. The WB bands were quantified with “Image Lab” software (Bio-Rad, Milan, Italy).

Determination of ploidy

Cells were treated with 0.2 μg/ml colcemid (Demecolcine, Sigma-Aldrich, Milan, Italy) for 4 h, harvested by trypsinization, swollen in 75 mM KCl at 37 °C, fixed with 3:1 methanol/acetic acid (v/v), and dropped onto clean, icecold glass microscope slides. The slides were air-dried and stained with 3% GIEMSA in phosphate-buffered saline for 10 min. Chromosome numbers were evaluated by quantifying 50 metaphases for each sample under a 63× objective using a Zeiss Axioskop microscope. Cytogenetic experiments were performed fourfold and threefold for IMR90 and HCT116 cells, respectively. A Student’s t test was performed to assess significance.

Immunofluorescence microscopy

To visualize β-tubulin, cells were grown on rounded glass coverslips and then fixed with Ethanol/Acetic acid 95:5 for 10 min, permeabilized with 0.1% TritonX (Sigma-Aldrich, Milan, Italy) in PBS for 15 min and blocked with 0.1% Bovine Serum Albumin (BSA) for 30 min. The procedure was carried out at room temperature. Coverslips were incubated with a mouse monoclonal antibody against β-tubulin mouse (1:200, Sigma-Aldrich, Milan, Italy) overnight at 4 °C, followed by incubation with a goat anti-mouse IgG FITC secondary antibody (Sigma-Aldrich, Milan, Italy; diluted 1:100 in PBS) for 1 h at 37 °C. Nuclei were visualized with 1 mg/ml of 40,6-Diamidino-2-phenylindole (DAPI) and examined under a Zeiss Axioskop microscope equipped for fluorescence. Images were captured with a CCD digital camera (AxioCam, Zeiss, Milan, Italy) and analyzed with Adobe Photoshop. We evaluated at least 100 mitoses for each sample. To visualize $p14^{ARF}$, HCT116 cells were stained with a goat polyclonal antibody against $p14^{ARF}$ (C-18, Santa Cruz Biotechnology, diluted 1:100) and incubated with FITC-conjugated donkey anti-goat IgG (Santa Cruz Biotechnology, diluted 1:200) for 1 h at 37 °C. To visualize CENP-E, IMR90 and HCT116 cells were stained with a mouse monoclonal antibody against CENP-E (C-5, Santa Cruz Biotechnology, diluted 1:100) and incubated with FITC-conjugated anti-mouse IgG (Sigma-Aldrich, diluted 1:200) for 1 h at 37 °C.

Cell cycle phase analysis PI staining and cytofluorimetric analysis

Cell cycle stage was analysed by flow cytometer using a Propidium Iodide (PI) staining assay based on the bind of PI, a DNA dye that bind the DNA in a stoichiometric way (it bind in proportion to the amount of DNA present in the cell), so it is possible to resolve cell cycle phases in a given cell population into G0/G1, S, and G2/M phases. Aliquots of 10,000,000 cells were harvested by centrifugation, washed with PBS and incubated in the dark in a PBS solution containing 20 mg/ml propidium iodide and 200 mg/ml RNase, for 30 min, at room temperature. Then, samples were immediately subjected to fluorescence-activated cell sorting

analysis by Epics XLe flow cytometer using Expo32 software (Beckman Coulter). At least 10,000 cells were analysed for each sample.

Gene expression microarray analysis

Total RNA was extracted from IMR90 cells after 72 hours of transfection as previously described. The quantity and purity of RNA samples were measured using the NanoDrop ND-1000 spectrophotometer (NanoDrop Technologies, Inc., Rockland, Del., USA), the integrity in ribosomal RNA 18S and 28S bands was also observed using the Agilent 2100 Bioanalyzer with an RNA 6000 Nano LabChip Kit. Total RNA (1 μg) of each sample or control was labelled with the Quick-Amp labeling kit (Agilent Technologies) to generate fluorescent cRNA (Fig.36). The samples and controls were both labelled with the fluorophores Cy3 and Cy5 in two separated reaction mixtures, in order to perform hybridizations in dye-swap. RNA spike-ins were mixed with the experiment sample during preparation. Known amounts of RNA Spike-In A and B (Agilent technologies) were mixed with samples during preparation, respectively to Cy3 labelled reaction mixture and Cy5 labeled reaction mixture, as control to calibrate measurements in a DNA microarray experiment. Subsequently the measured degree of hybridization between the spike-ins and the control probes was used to normalize the hybridization measurements of the sample RNA. The quality of the labelled cRNA, its concentration and incorporation efficiency of the two cyanines were evaluated spectrophotometrically at NanoDrop ND-1000 with an appropriate software. The same amount of sample and respective control, differentially labelled and corresponding to not less than 5.0 pmol of cyanine dyes, were brought together in a single hybridization mixture, subjected to fragmentation and then hybridized on Whole Human Genome 4X44K array, containing unique probes corresponding to ~41,000 human genes, manufactured by Agilent (G4114F, Agilent Technologies). Each hybridization was carried out in order to compare the samples with the selected control, and each experiment was performed in dye- swap (as previously describe) hybridization to reduce the variability due to the possible incorporation of the two different cyanine dyes. After an incubation of 17 hours at 65°C, the slides were washed with the Gene Expression Wash Buffer Kit (Agilent Technologies) and analyzed with the dual-laser microarray scanner Agilent B (Agilent Technologies) at 5 μm of resolution. The images obtained were analyzed using the Feature Extraction software version 8.3 (Agilent Technologies).

Statistical data analysis, background correction, normalization and summary of expression measure were conducted with GeneSpring GX ver. 12.0 (Agilent, Santa Clara, CA, USA). Data were filtered using two-step procedure: first the entities were filtered based on their flag values P (present) and M (marginal) and then filtered based on their signal intensity values. Statistically significant differences were computed by the Student's t-test and the significance level was set at $p<0.05$. The false discovery rate (FDR) was applied as a multiple test correction method. Unsupervised hierarchical clustering was performed using the Euclidean distance and the average linkage method. Differentially expressed genes (DEGs) were selected by a supervised approach using the ANOVA package. Formally, a contrast fold change of at least ±1.5 and an FDR corrected p-value <0.05 was used in order to perform multiple pairwise comparisons between each class (siCENPE 72h and siCENPE 2w) and the control (siGFP).

Gene Set Enrichment Analysis (GSEA)

Normalized expression ratio data for the siRNA treated IMR90 cells vs siGFP treated IMR90 cells contrast were further analyzed using the Gene Set Enrichment Analysis (GSEA) method 18. GSEA is a computational method that determines if an priori defined set of genes indicates statistically significant between two phenotypes. In GSEA, genes are ranked by their correlation with phenotype and every enrichment gene set will get an enrichment score (ES). 1000 gene permutations were used to generate a null distribution for ES, then each pathway will attain a normalization enrichment score (NES). H: Hallmark and C5:BP:GO biological process, including 4486 gene sets, were used as gene sets database. Gene sets were considered significantly enriched with q-value < 0.1 and p-value < 0.005.

REFERENCES

Abrieu, Ariane, et al. "CENP-E as an essential component of the mitotic checkpoint in vitro." Cell 102.6 (2000): 817-826.

Balamuth, Naomi J., et al. "Serial transcriptome analysis and cross-species integration identifies centromere-associated protein E as a novel neuroblastoma target." Cancer research 70.7 (2010): 2749-2758.

Barisic, Marin, et al. "Kinetochore motors drive congression of peripheral polar chromosomes by overcoming random arm-ejection forces." Nature cell biology 16.12 (2014): 1249.

Bennett, Ailsa, et al. "Cenp-E inhibitor GSK923295: Novel synthetic route and use as a tool to generate aneuploidy." Oncotarget 6.25 (2015): 20921.

Boveri T., 1902 Uber mehrpolige Mitosen als Mittel zur Analyse des Zellkerns. Verhandlungen der physikalisch-medizinischen Gesellschaft zu Wu¨rzburg. Neu Folge 35: 67–90.

Boveri, T., 1904 Ergebnisse uber die Konstitution der Chromatischen Substanz des Zellkerns. Gustav Fischer, Jena, Germany.

Britigan, Eric MC, et al. "The ARF tumor suppressor prevents chromosomal instability and ensures mitotic checkpoint fidelity through regulation of Aurora B." Molecular biology of the cell 25.18 (2014): 2761-2773.

Brown, Kevin D., et al. "Cyclin-like accumulation and loss of the putative kinetochore motor CENP-E results from coupling continuous synthesis with specific degradation at the end of mitosis." The Journal of Cell Biology 125.6 (1994): 1303-1312.

Bunz, F. et al., 2002. Targeted inactivation of p53 in human cells does not result in aneuploidy. Cancer research, 62(4), pp.1129–33.

Chen, D. et al., 2005. ARF-BP1/Mule is a critical mediator of the ARF tumor suppressor. Cell, 121(7), pp.1071–83.

Chunduri, Narendra Kumar, and Zuzana Storchova. "The diverse consequences of aneuploidy." Nature cell biology 21.1 (2019): 54.

Cimini, Daniela, and Francesca Degrassi. "Aneuploidy: a matter of bad connections." Trends in cell biology 15.8 (2005): 442-451.

Cleveland, Don W., Yinghui Mao, and Kevin F. Sullivan. "Centromeres and kinetochores: from epigenetics to mitotic checkpoint signaling." Cell 112.4 (2003): 407-421.

Collin, Philippe, et al. "The spindle assembly checkpoint works like a rheostat rather than a toggle switch." Nature cell biology 15.11 (2013): 1378.

Dick, Amalie E., and Daniel W. Gerlich. "Kinetic framework of spindle assembly checkpoint signalling." Nature cell biology 15.11 (2013): 1370.

Dobles, Max, et al. "Chromosome missegregation and apoptosis in mice lacking the mitotic checkpoint protein Mad2." Cell 101.6 (2000): 635-645.

Dürrbaum, Milena, et al. "Unique features of the transcriptional response to model aneuploidy in human cells." BMC genomics 15.1 (2014): 139.

Eymin, B. et al., 2003. p14ARF induces G2 arrest and apoptosis independently of p53 leading to regression of tumours established in nude mice. Oncogene, 22(12), pp.1822–35.

Eymin, B. et al., 2006. p14ARF activates a Tip60-dependent and p53-independent ATM/ATR/CHK pathway in response to genotoxic stress. Molecular and cellular biology, 26(11), pp.4339–50.

El-Arabey, Amr Ahmed, Salama Abdu Salama, and Adel Rashad Abd-Allah. "CENP-E as a target for cancer therapy: Where are we now?." Life sciences 208 (2018): 192-200.

Foijer, Floris, Viji M. Draviam, and Peter K. Sorger. "Studying chromosome instability in the mouse." Biochimica et Biophysica Acta (BBA)-Reviews on Cancer 1786.1 (2008): 73-82.

Giam, Maybelline, and Giulia Rancati. "Aneuploidy and chromosomal instability in cancer: a jackpot to chaos." Cell division 10.1 (2015): 3.

Gordon, David J., Benjamin Resio, and David Pellman. "Causes and consequences of aneuploidy in cancer." Nature Reviews Genetics 13.3 (2012): 189.

Granic, Antoneta, and Huntington Potter. "Mitotic Spindle Defects and Chromosome Mis-Segregation Induced by LDL/Cholesterol—Implications for Niemann-Pick C1, Alzheimer's Disease, and Atherosclerosis." PLoS One 8.4 (2013): e60718.

Gudimchuk, Nikita, et al. "Kinetochore kinesin CENP-E is a processive bi-directional tracker of dynamic microtubule tips." Nature cell biology 15.9 (2013): 1079.

Gudimchuk, Nikita, et al. "Probing mitotic CENP-E kinesin with the tethered cargo motion assay and laser tweezers." Biophysical journal 114.11 (2018): 2640-2652.

Haindl, M. et al., 2008. The nucleolar SUMO-specific protease SENP3 reverses SUMO modification of nucleophosmin and is required for rRNA processing. EMBO reports, 9(3), pp.273–9.

Hibi, Kenji, et al. "Methylation of the TFPI2 gene is frequently detected in advanced gastric carcinoma." Anticancer research 30.10 (2010): 4131-4133.

Holland, Andrew J., and Don W. Cleveland. "Boveri revisited: chromosomal instability, aneuploidy and tumorigenesis." Nature reviews Molecular cell biology 10.7 (2009): 478.

Huang, L. Eric, et al. "Hypoxia-induced genetic instability—a calculated mechanism underlying tumor progression." Journal of Molecular Medicine 85.2 (2007): 139-148.

Ko, Aram, Su Yeon Han, and Jaewhan Song. "Regulatory network of ARF in cancer

development." Molecules and cells 41.5 (2018): 381.

Kondoh, Miyako, et al. "Hypoxia-induced reactive oxygen species cause chromosomal abnormalities in endothelial cells in the tumor microenvironment." PloS one 8.11 (2013): e80349.

Kops, Geert JPL, Beth AA Weaver, and Don W. Cleveland. "On the road to cancer: aneuploidy and the mitotic checkpoint." Nature Reviews Cancer 5.10 (2005): 773.

Lara-Gonzalez, Pablo, Frederick G. Westhorpe, and Stephen S. Taylor. "The spindle assembly checkpoint." Current biology 22.22 (2012): R966-R980.

Lee, Alvin JX, et al. "Chromosomal instability confers intrinsic multidrug resistance." Cancer research 71.5 (2011): 1858-1870.

Lentini, Laura, et al. "MAD2 depletion triggers premature cellular senescence in human primary fibroblasts by activating a p53 pathway preventing aneuploid cells propagation." Journal of cellular physiology 227.9 (2012): 3324-3332.

Lentini, Laura, et al. "Simultaneous reduction of MAD2 and BUBR1 expression induces mitotic spindle alterations associated with p53 dependent cell cycle arrest and death." Cell biology international 38.8 (2014): 933-941.

Li, Min, et al. "Loss of spindle assembly checkpoint–mediated inhibition of Cdc20 promotes tumorigenesis in mice." The Journal of cell biology 185.6 (2009): 983-994.

Maggi, L.B. et al., 2014. ARF tumor suppression in the nucleolus. Biochimica et Biophysica Acta (BBA) - Molecular Basis of Disease, 1842(6), pp.831–839.

Mao, Y., Desai, A. & Cleveland, D.W., 2005. Microtubule capture by CENP-E silences BubR1-dependent mitotic checkpoint signaling. The Journal of cell biology, 170(6), pp.873–80.

McGranahan, Nicholas, et al. "Cancer chromosomal instability: therapeutic and diagnostic challenges." EMBO reports 13.6 (2012): 528-538.

Meraldi, Patrick, and Peter K. Sorger. "A dual role for Bub1 in the spindle checkpoint and chromosome congression." The EMBO journal 24.8 (2005): 1621-1633.

Musacchio, Andrea. "The molecular biology of spindle assembly checkpoint signaling dynamics." Current biology 25.20 (2015): R1002-R1018.

Nicholson, Joshua M., and Daniela Cimini. "How mitotic errors contribute to karyotypic diversity in cancer." Advances in cancer research. Vol. 112. Academic Press, 2011. 43-75.

Ozenne, P. et al., 2010. The ARF tumor suppressor: structure, functions and status in cancer. International journal of cancer, 127(10), pp.2239–47.

Pollice, A., Vivo, M. & La Mantia, G., 2008. The promiscuity of ARF interactions with the proteasome. FEBS letters, 582(23–24), pp.3257–62.

Pomerantz, J. et al., 1998. The Ink4a tumor suppressor gene product, p19Arf, interacts with MDM2 and neutralizes MDM2's inhibition of p53. Cell, 92(6), pp.713–23.

Rieder, Conly L., and Helder Maiato. "Stuck in division or passing through: what happens when cells cannot satisfy the spindle assembly checkpoint." Developmental cell 7.5 (2004): 637-651.

Saporita, A.J. et al., 2007. Therapeutic targets in the ARF tumor suppressor pathway. Current medicinal chemistry, 14(17), pp.1815–27.

Schaar, B.T. et al., 1997. CENP-E function at kinetochores is essential for chromosome alignment. The Journal of cell biology, 139(6), pp.1373–82.

Schvartzman, Juan-Manuel, Rocio Sotillo, and Robert Benezra. "Mitotic chromosomal instability and cancer: mouse modelling of the human disease." Nature Reviews Cancer 10.2 (2010): 102.

Sharpless, Norman E., and Ronald A. DePinho. "The INK4A/ARF locus and its two gene products." Current opinion in genetics & development 9.1 (1999): 22-30.

Sheltzer, Jason M., et al. "Transcriptional consequences of aneuploidy." Proceedings of the National Academy of Sciences 109.31 (2012): 12644-12649.

Sheltzer, Jason M., and Angelika Amon. "The aneuploidy paradox: costs and benefits of an incorrect karyotype." Trends in Genetics 27.11 (2011): 446-453.

Siegel, J.J. & Amon, A., 2012. New insights into the troubles of aneuploidy. Annual review of cell and developmental biology, 28, pp.189–214.

Silk, Alain D., et al. "Chromosome missegregation rate predicts whether aneuploidy will promote or suppress tumors." Proceedings of the National Academy of Sciences 110.44 (2013): E4134-E4141.

Simonetti, Giorgia, et al. "Aneuploidy: Cancer strength or vulnerability?." International journal of cancer 144.1 (2019): 8-25.

Smid, Marcel, et al. "Patterns and incidence of chromosomal instability and their prognostic relevance in breast cancer subtypes." Breast cancer research and treatment 128.1 (2011): 23-30.

Stingele, Silvia, et al. "Global analysis of genome, transcriptome and proteome reveals the response to aneuploidy in human cells." Molecular systems biology 8.1 (2012).

Thompson, Sarah L., Samuel F. Bakhoum, and Duane A. Compton. "Mechanisms of chromosomal instability." Current biology 20.6 (2010): R285-R295.

Torres, E.M. et al., 2007. Effects of aneuploidy on cellular physiology and cell division in haploid yeast. Science (New York, N.Y.), 317(5840), pp.916–24.

Van Jaarsveld, Richard H., and Geert JPL Kops. "Difference makers: chromosomal instability versus aneuploidy in cancer." Trends in cancer 2.10 (2016): 561-571.

Van Maerken, Tom, et al. "Escape from p53-mediated tumor surveillance in neuroblastoma: switching off the p14 ARF-MDM2-p53 axis." Cell death and differentiation 16.12 (2009): 1563.

Veneziano, Lorena, et al. "p14ARF Prevents Proliferation of Aneuploid Cells by Inducing p53-Dependent Apoptosis." Journal of cellular physiology 231.2 (2016): 336-344.

Weber, J.D. et al., 1999. Nucleolar Arf sequesters Mdm2 and activates p53. Nature cell biology, 1(1), pp.20–6.

Weaver, Beth AA, et al. "Aneuploidy acts both oncogenically and as a tumor suppressor." Cancer cell 11.1 (2007): 25-36.

Wilson, Matthew H., Craig J. Coates, and Alfred L. George Jr. "PiggyBac transposon-mediated gene transfer in human cells." Molecular therapy 15.1 (2007): 139-145.

Wood, Kenneth W., et al. "Antitumor activity of an allosteric inhibitor of centromere-associated protein-E." Proceedings of the National Academy of Sciences 107.13 (2010): 5839-5844.

Yamagishi, Yuya, et al. "Kinetochore composition and its function: lessons from yeasts." FEMS microbiology reviews 38.2 (2014): 185-200.

Yen, T.J. et al., 1992. CENP-E is a putative kinetochore motor that accumulates just before mitosis. Nature, 359(6395), pp.536–9.

Yu, Kai-Wei, et al. "Mechanisms of kinesin-7 CENP-E in kinetochore–microtubule capture and chromosome alignment during cell division." Biology of the Cell (2019).

SOMMARIO